Winter 2018

Dynamic Response Modeling of High Speed Planing Craft with Enforced Acceleration

Brian K. Johnson
Old Dominion University, bkeithjohn1@yahoo.com

DYNAMIC RESPONSE MODELING OF HIGH SPEED PLANING CRAFT WITH ENFORCED ACCELERATION

by

Brian K. Johnson
B.S.M.E December 2015, Old Dominion University

A Thesis Submitted to the Faculty of
Old Dominion University in Partial Fulfillment of the
Requirements for the Degree of

MASTER OF SCIENCE

MECHANICAL ENGINEERING

OLD DOMINION UNIVERSITY
December 2018

Approved by:

Gene Hou (Co-Director)

Jennifer Michaeli (Co-Director)

Miltos Kotinis (Member)

ABSTRACT

DYNAMIC RESPONSE MODELING OF HIGH SPEED PLANING CRAFT WITH ENFORCED ACCELERATION

Brian K. Johnson
Old Dominion University, 2018
Co-Directors: Dr. Gene Hou
Dr. Jennifer Michaeli

Due to the harsh conditions high speed planing crafts must endure, research to further the understanding of high speed vessel response during wave impacts was conducted. The integration of a finite element model and captured sea trial acceleration data was investigated. The research shows that the finite element model sub-model can be used in lieu of a full finite element model with minimum degradation in output, thus allowing for the analysis of local stress concentrations where critical equipment and or personnel may be located.

The research effort was completed to develop a method for realizing the stress field and deformation generated following a wave impact. Application of base excitation was investigated and allowed for multiple studies to be completed. Validation of the method was accomplished through comparison of sea trial data with MSC NASTRAN transient response output in the form of acceleration. The method provides insight into the effect that wave impacts have on small vessels at sea, specifically the 11-meter cabin RIB, hull 11MRIB0503.

This thesis is dedicated to everyone who has taken time to share their knowledge with me. Thank you all.

ACKNOWLEDGMENTS

I would like to thank Dr. Jennifer Michaeli for introducing me to the work being conducted at Naval Surface Warfare Centers. Her collaboration with the warfare centers allowed me to gain real world experience not available at all universities.

I would like to thank Dr. Gene Hou for continuing to provide technical advice and guidance on this research effort. His passion for research is always encouraging. His knowledge and expertise has been greatly appreciated.

I would like to thank Heidi Murphy, Chris Planchak, and Dr. Tim Coats with NSWC Carderock, Combatant Craft Division, Test & Evaluation Branch, for conducting the testing and making the data available.

Finally, I would like to thank Mr. John Zseleczky at U.S. Naval Academy for providing access to the StandardG software.

TABLE OF CONTENTS

Page

LIST OF TABLES viii

LIST OF FIGURES ix

Chapter

1. INTRODUCTION 1

1.1 Motivation 1
1.2 Objectives 1
1.3 Approach 3

2. BACKGROUND 5

2.1 Literature Review 5
2.2 Supplied Data 11
2.2.1 Finite Element Model 11
2.2.2 Acceleration Data 14
2.2.3 StandardG Algorithm 15

3. DYNAMIC RESPONSE MODELING OF A HIGH SPEED PLANING CRAFT WITH ENFORCED ACCELERATION 18

3.1 Equation of Motion under Base Excitation 18
3.2 PATRAN and NASTRAN Solution Procedure for Enforced Acceleration 20
3.3 Full Boat Validation 21

4. ENGINEERING APPLICATIONS 37

4.1 Sensitivity Study 37
4.2 Displacement 40
4.3 Cabin Sub-model Analysis 42

5. CONCLUSION AND RECOMMENDATIONS 53

Page

REFERENCES 55

Appendix A – PATRAN and NASTRAN Enforced Acceleration Procedure 60

Appendix B – MATLAB Data Plots 66

Appendix C – Deformation Plots 67

Appendix D – Approximation Validation Plots 70

VITA 73

LIST OF TABLES

Table Page

1. FEM Nastran Elements 12

2. MSC Nastran Modal Sample Results (Trenor et al., 2015) 13

3. Completed Seakeeping Runs 14

4. Accelerometer Locations on 11-meter Cabin RIB 25

5. Envelope Deviation (g's): 11 Accelerometers as Input 35

6. Filtered Subcase 3 of Constant Speed Envelope Deviation (g's): Reduced Number of Accelerometers as Input 38

7. Filtered Data Percent Difference 39

LIST OF FIGURES

Figure Page

1. Rigid Body Motion and Structural Flexure (Riley & Coats, 2013) 16

2. Peak Extraction Plot from Accelerometer 11Z 17

3. MSC NASTRAN Acceleration Input Flowchart 20

4. Full Boat Validation Flowchart 22

5. Subcase 3 of Constant Speed Envelope: Accelerometer 1Z Raw Data Plot 23

6. Subcase 3 of Constant Speed Envelope: 1Z Full Boat Spectrum Plot 23

7. Side-View of 11-meter Cabin RIB Model with Accelerometer Locations 26

8. Top-View of 11-meter Cabin RIB Model with Accelerometer Locations 26

9. Filtered Constant Speed Envelope 30

10. Filtered Constant Wave Height Envelope 32

11. Filtered Maximum Safe Speed Envelope 34

12. Filtered Comparisons after Accelerometers 8Z and 9Z Deleted 39

13. Side View of Deformation plot at 0.31 seconds 41

14. Top View of Deformation plot at 0.31 seconds 41

15. Isolated Pilot Cabin 42

16. Subcase 3 of Constant Speed Envelope: 16Z Pilot Cabin Spectrum Plot 43

17. Side-View of 11-meter Cabin RIB Model Transverse Bulkheads 45

18. Seven Node Locations on 11-meter Cabin RIB Model 45

19. Pilot Cabin Output Comparison with Data Filtered at 10 Hertz 47

20. Pilot Cabin Output Comparison with Data Filtered at 13 Hertz 47

21. Stress Contour Plot using Data Filtered at 13 Hertz: Z2 Maximum Stress 48

Figure Page

22. Stress Contour Plot using Data Filtered at 13 Hertz: Z1 Maximum Stress 48

23. Node 5838 and Node 4957 Acceleration Plots 49

24. Node 5838 and Node 4957 Stress Plots 50

25. Cabin Stress Contour Plot at Z2: Port Seat Pedestal Node 5838 51

26. Cabin Stress Contour Plot at Z1: Port Seat Pedestal Node 5838 51

27. Cabin Stress Contour Plot at Z2: Starboard Seat Pedestal Node 4957 52

28. Cabin Stress Contour Plot at Z1: Starboard Seat Pedestal Node 4957 52

CHAPTER 1

1. INTRODUCTION

This chapter is dedicated to the discussion of the motivation behind the research effort, objectives, and the approach taken to complete the study.

1.1 Motivation

Over the years, researchers have investigated the effects that different sea conditions have on sea vessels. Sloshing, green water, and slamming are transient excitations that occur during said sea conditions and can be detrimental to at sea performance. In addition to sea conditions, hull form greatly effects how a vessel is able to move through the water. Small fast vessels are usually equipped with planing hulls to increase speed. The planing hull will generate locally high hydrodynamic pressure in high speed so as to reduce friction drag and wave resistance. Unfortunately, a planing hull craft often encounters high slamming loads with high encountering frequency. Such slamming can suddenly alter sailing direction and speed. In addition to operability challenges, the high g-forces encountered while aboard a high speed planing craft are known to be harmful to the individuals aboard. The combination of craft speed and wave height creates hazardous conditions, not only for those individuals aboard but also for the traversing sea vessel itself, from boat hull to onboard equipment. In order to mitigate risk, it is important that steps are taken to ensure the sea vessel is structurally sound for the safety of the warfighters.

1.2 Objectives

The objectives of this investigation were multi-fold. Provided with a finite element model, built by Naval Surface Warfare Center Carderock Division, Detachment Norfolk (NSWCCD DN) Code 60 personnel using commercial code FEMAP, Old Dominion University researchers investigated the feasibility of using commercial code PATRAN and MSC NASTRAN to validate

the finite element model against data collected during multiple NSWCCD Code 80 sea trials. The procedures discussed, can be carried out to provide insight into how well a finite element model represents actual events at sea without finding the actual wave loads.

The first objective of this work was to validate the finite element model built by NSWCCD Code 60 through transient analysis. The transient analysis was completed using full-scale vertical acceleration data collected by NSWCCD Code 80. The second objective was to investigate the effect of number and placement of accelerometers used for enforced excitation. The third objective was to investigate the effects of enforced excitation on the pilot cabin.

With continued advances in technology, institutions, more than ever, have the ability to take advantage of modeling and simulation software tools. However, errors in input can easily lead to misleading information. Therefore, it is important that proper methods be used during the application of such software tools within a study. With a well-defined and tested procedure, multiple institutions can adopt, compare results, and contribute. If the representation is accurate, insight into the local and global stress and displacement are obtainable, as will be shown.

This study provides the community of interest with a procedure for modeling the effects of wave impact. Through simulation, visualization of the effects of changing said accelerometer inputs and filtering parameters is achievable.

This work provides an acceleration load input method for finite element based dynamic analysis of a seagoing vessel. The study will show the integration of a finite element model with acceleration data to approximate stress and displacement values in the absence of strain gauges, pressure transducers, or computational fluid dynamics models employed in other model based research efforts. It is shown how this approximation method is considered adequate for analysis of the cabin region. The cabin is of interest as numerous research efforts have been conducted for

seat mitigation and have stated the hazard to shipboard equipment but lack the recorded data from strain gauges or pressure transducers. The integration will provide additional insight into the effect of wave impact on a high speed planing craft.

In order to broaden the knowledge base on the finite element analysis software utilized by the Naval Engineering and Marine Systems Institute, both results and procedures are discussed. The compilation of research conducted in this field of study will facilitate researchers interested in base excitation, model validation, and finite element analysis. In addition to multiple research interests, this document is meant to serve as a manual for conducting transient analysis. Therefore, instructional reference material on how to implement investigations using the PATRAN and MSC NASTRAN software was outlined in Appendix A.

Overall, the benefit of this research is to show that a smaller amount of data, both accelerometers and model size, are able to provide beneficial insight into the effect that sea states have on equipment and personnel out at sea. The method applied can provide advice on where bulkhead accelerometers should be located to analyze the entire cabin. This way, less time is spent developing a full model, and the areas of most concern such as warfighter seats and critical cabin equipment can be analyzed for design improvements.

1.3 Approach

Over the years, researchers have investigated the effects that different sea states have on sea vessels. The interest in predicting hull transformations over the course of vessel use has led to the application of empirical equations, theoretical models, and small-scale simulations. This research effort was initiated to show how acceleration data can be leveraged by researchers to predict the location of stress concentrations due to wave slamming. The application is driven by the method known as base excitation. Acceleration data was used as direct input during transient

analysis to observe the resulting stress along the sea vessel, specifically the cabin space, where the warfighter may be located during travel. The use of acceleration as an input was validated by enforcing acceleration data about specific nodes and recording the resulting acceleration output at the bottom, midsection, and top of the pilot cabin. The resulting acceleration was then compared to the acceleration output from sea trials.

In order to accomplish the three objectives previously discussed, multiple investigations were completed. The investigations are detailed in the order in which they appear in the current work. First, a literature review of previous research conducted regarding enforced acceleration analysis and high speed planing crafts was completed. Second, finite element model validation through forced excitation and comparison to sea trial data was completed. Third, an investigation of quantity and placement for forced acceleration input using sea trial data was conducted. Fourth, enforced acceleration through isolated pilot cabin was completed.

In order to provide guidance, the scope of this thesis is briefed. The literature review is discussed in Chapter 2. The finite element model validation is discussed in Chapter 3. The investigation into quantity and placement of accelerometers is detailed in Chapter 4. Enforced acceleration through isolated pilot cabin was completed in Chapter 4. The thesis conclusion and recommendations are provided in Chapter 5.

CHAPTER 2

2. BACKGROUND

This chapter is dedicated to the discussion of the literature reviewed to form the basis of this research effort and the supplied data utilized during the completion of this research effort.

2.1 Literature Review

The slamming phenomena of a planing hull involves fully coupled dynamic interaction between fluid, structure, wind, wave, and the vessel itself. To fully understand the slamming phenomena and its consequences on the design and operation of a planing hull is very challenging and has drawn the attention of many researchers in the past. To aid these efforts, many drop tests of wedges, towing tank tests, sea trails, and numerical simulations have been conducted to collect the data on point accelerations, pressures, and strains on the planing hull. Based upon the collected data, Allen, Jones & Taylor (1978) introduced a semi-empirical equation that correlates the impact pressure to the value of the 1/10th highest peak vertical acceleration. The value of the 1/10th highest peak vertical acceleration can be experimentally measured or approximated in terms of wave height, forward speed, and geometry features of the boat (Hoggard & Jones, 1980). Similar semi-empirical equations with different levels of average acceleration have been developed and incorporated in design and safety rules, chosen by the classification societies such as American Bureau of Shipping (ABS), Det Norske Veritas (DNV), or Lloyd's Register (Grimsley, Liu, & Hou, 2010). The exponential distribution has been wildly used, which was suggested early by Fridsma (1971), to estimate different levels of the averaged acceleration based upon the same set of statistical parameters of the collected acceleration time series.

Recent studies have cautioned the use of the Allen and Jones' equation. These new investigations have come about by conducting new experiments or by numerical simulation. Riley et al. (2010, 2016) have pointed out the need of standardizing the definition of a slamming event so as to better characterize acceleration data. Razola et al. (2014) improved the accuracy of the Allen and Jones' equation by modifying the existing load-carrying area aspect ratio and adding a new one, the load transverse reduction factor. Furthermore, some researchers have questioned the use of the exponential distribution to quantify the peak acceleration data (Razola, et al. 2016; VanDerwerken & Judge, 2017). Others have called for a dynamic structural analysis of a planing hull in a slamming event. Rozola et al. (2014) indicated that to design a planing hull serving for a long life requires the understanding of local deformation and stresses under extreme slamming pressure. Joo et al. (2017) and Riley & Petersen (2017) pointed out the need of a pointwise impulse acceleration profile right under a crew seat or an on-board equipment are important for the design of a suitable shock isolation mount for crew and operation safety. These additional design requirements of a safe and robust planing hull require, not only the average design pressure, but the detailed structural responses in time of the boat at various concerned locations. This requires a detailed dynamic structural analysis of the flexible boat in a slamming event.

Full simulation of a slam impact event for a planning hull is still under development, though significant advancement has been made recently. The challenges lie on its multidisciplinary nature, which requires intensive modeling and computation efforts. The emerging approach is to develop a unified set of governing differential equations to cover all involved disciplines which are then solved with a unified numerical mesh and algorithm. This approach is called closely coupled approach (Hou et al., 2012). Yang (2018) studied the breaking

water generated due to an impact generated by a free fall rigid body. He modeled three different domains: air, fluid, and rigid body, in the same form of Navier-Stokes equation in which the velocity and the pressure are the unknowns. This method has yet to be extended to planing hulls.

As mentioned previously, the current approach is called loosely coupled approach (Yang & Huang, 2016). At each time instance, the approach uses separately developed numerical models to simulate waves, fluid, and vessel structure individually. Then, their solutions are reconciled based upon the common conditions, before moving on to the next time step. The main challenges of this approach lie on the difficulties to accurately trace the location of the moving boundary and transfer boundary velocity and pressure between different domains with different meshes. Various methods such as overset grids (Sukas et al., 2017) and immersed method (Yang, 2018) have been studied to overcome such issues of mismatched meshes.

Ma and Mahfuz (2012) simulated the heave and pitch of a multi-hull ship model moving with a constant forward speed in a water tank. Its hull panel, girders, and web frames were made of sandwich composite panels. The entire structure was discretized with 3,247 nodes and 3,162 shell elements. ANSYS was used for a coupled fluid and structural analysis, incorporated with harmonic surface waves simulated by a 2D potential flow model. Their results demonstrated that it is important to take the elastic deformation into account in the FSI analysis as it affects the fluid pressure distribution around the ship hull. To further study the detailed failure modes in the web-girder interface, the authors first identified the high stress area from the global FSI analysis which was carried out based on a coarse mesh. The local sub-model was then established around the high stressed area with refined meshes. The quasi-static analysis of the sub-model was then analyzed, subjected to the force and displacement values obtained in the global FSI analysis. Xie et al. (2018), investigated a water-entry hydro-elastic problem using FLUENT for fluid dynamics

simulation, ANSYS for structural analysis, and the volume of fluid method for air-water interface. A constrained minimization was constructed to convert the element center pressure output from FLUENT to nodal pressure input to ANSYS. The simulation results compared satisfactorily with water entrance testing data.

Stern and his colleagues used their comprehensive CFDSHIP-IOWA, which models the viscous fluid domain with a moving interface boundary between the vessel and the fluid and models the free surface with level set method. The surface pressure was collected to simulate the motion of the vessel, which in turn altered the fluid domain boundary. Overset gridding was used for data transfer between interfaced domains. This method enables visualization of physics details in fluid-structure interaction (Carrica et al., 2010). However, this method is computationally intensive. In their recent work, elastic deformation was considered only for part of the ship hull and solved by ANSYS finite element code (Volpi et al., 2017). The results compared favorably with the testing results in sea trials. Alternatively, fluid-structure interaction in time domain was carried out for a rigid vessel. The instantaneous surface pressure was then applied to the finite element model of the flexible vessel to find the dynamic responses in a quasi-static state (Volpi et al., 2017; Faltinsen, 2005).

The studies of Garme, Rosen, and their colleagues (Garme & Rosen, 2003; Rozola et al., 2014; 2016), focused on the motion profile of the planing hull. The approach they used may be termed as a single disciplinary approach. They solved only the equation of motion of a rigid planing hull for surging, heaving, and pitching subjected to the loads integrated from time dependent sectional pressures. These sectional pressures were evaluated based upon the nonlinear strip theory, which was derived from a potential flow model for vertical impact of a 2D wedge. The advantage of this approach is its computational efficiency which enables the research

team to conduct numerical simulations for a long period of time so as to quantify the statistical nature of the acceleration time series. In their study, they pointed out the importance of maximal displacement and stress of panels for the lifelong design of a planing hull. These local structure responses are the result of local extreme pressure during slamming applied to the flexible boat hull, not the averaged design pressure. To address this issue, they (Rozola et al., 2014) built a finite element model of a section of a boat hull. Structure dynamic analysis was conducted then for the modeled section subjected to pressure distribution reconstructed from the pressure data collected from 12 pressure transducers. The pressure distribution reconstruction strategy was derived based upon the assumption that the fluid particle moves with the same speed from the keel to the chine on a section of the planing hull (Rosen & Garme, 2004; Rosen, 2005).

The single disciplinary approach will be employed in this paper to investigate structural dynamic response of a planing hull slamming event. However, in this study, instead of pressure transducers, the data collected from accelerometers will be used as enforced excitation to simulate the slamming loads. Enforced excitation referred here is a type of dynamic response induced by the prescribed time-dependent boundary conditions prescribed in terms of displacement, velocity, or acceleration. Structural analysis through enforced excitation has been conducted on structures in the air and on the ground alike, most notably in the analysis of space shuttle main engine structures and the induced vibration of structures during earthquakes or on a shaker table. The large mass method is commonly used to enforce a single-degree boundary motion, in which the excitation force is equal to the acceleration multiplied by the mass value (Clough & Penzien, 1975). Davis et al., (2012) simulated the drop test response of onboard equipment through the use of a 6 degree-of-freedom (DOF) motion simulator. The enforced base excitation method proved successful by validation through frequency and transient responses, in

which the input was the motion profile measured by a single base accelerometer. In a broader view, a structure under enforced excitation can be formulated as a differential-algebra equation, which can be solved by introducing Lagrange multipliers to impose the prescribed boundary motion. The resultant set of equations can be solved by the elimination method or the penalty method (Chandrupatla & Belegundu, 2012). The elimination method separates the displacements into the boundary set and the relative or the interior set (Cho et al., 2016; Flanigan, 1994; Bampton & Craig, 1968; Blades & Craig, 1997). The equation of motion of the entire structure is also reformulated into two. One is an ordinary differential equation solved for the interior or the relative displacements while the other is an algebra equation directly used to compute the value of the Lagrange multipliers. The penalty method has been commonly used in finite element problems for static structural analysis or dealing with incompressibility conditions in velocity-pressure flow problems (Reddy, 1984), though seldom used in the time-dependent problems. The work of Liu & Lu (2010) is an example which applied the penalty method to count for earthquake base excitation in seismic analysis of structures. Scovazzi et al., (2017) proposed an interesting approach, which not only achieves accurate velocity as well as stresses but accommodates easily with enforced velocity and stress boundary conditions. Their equation of motion is expressed in terms of the first order time derivatives of stresses and velocities.

This study will conduct the structural dynamic analysis of an 11-meter Rigid Inflatable Boat (RIB) under a slamming event. This is done by adopting the enforced motion analysis capability provided by the commercially available finite element analysis software, MSC NASTRAN, which is built upon the elimination approach.

2.2 Supplied Data

Two previous Navy warfare center research efforts formed the foundation from which the current study was able to build upon. The first research effort included the initial modeling of the 11-meter cabin RIB. The second research effort included sea trials on the 11-meter cabin RIB. A finite element model of the 11-meter cabin RIB, acceleration data from sea trials, and the StandardG algorithm were supplied to Old Dominion University in support of this study. An overview of the data each effort generated is discussed.

Furthermore, full-scale vertical acceleration data on an 11-meter cabin RIB was collected by NSWCCD for a range of speeds and significant wave heights and made available to Old Dominion University's Naval Engineering and Marine Systems Institute (NEMSI), along with a finite element model of the vessel.

2.2.1 Finite Element Model

In support of the Combatant Craft Division, NSWCCD Code 661 developed a finite element model of a Zodiac H1110 AFT IO CABIN RIB (Corbishdale, 2014). Modal analysis of the FEM was completed by Code 661 to aid the Combatant Craft Division selection of accelerometer placements before sea trials were conducted. The finite element model of the RIB was generated in FEMAP version 11.0, and NEiNASTRAN version 10.1 was used for modal analysis. Due to unknown material, properties, and weights, assumptions were made in the development of the finite element model (Corbishdale, 2014). A smearing technique was utilized to distribute the mass of more complex features, such as windows, doors, inflatable sponson, and fuel. The finite element model weight of 15, 320 lbf was achieved with a final smearing of 3,650 lbf over all primary structures (Corbishdale, 2014), which is consistent with the weight of the

actual planing craft. The elements used to build the finite element model, and their quantity, are provided in Table 1.

Table 1. FEM Nastran Elements

Element	Quantity
CBEAM	211
CONM2	4,372
CQUAD4	50,634
CTRIA3	798
RBE2	45

The longitudinal center of gravity (LCG) of the physical boat, as measured from the transom-keel intersection, was approximately 10.440 feet with an uncertainty of approximately $\pm$0.872 % (Murphy & Planchak, 2015). The finite element model of the boat had the LCG located at approximately 135 inches (11.25 feet) as measured from the transom-keel intersection (Murphy & Planchak, 2015). The difference between the LCG locations on the physical boat and finite element model is approximately 7.76 % which is well outside the uncertainty in the LCG measurement of the real-world boat.

It is important to note that sea trials were conducted with a weight of 15,845 lbf with the addition of crew, seats, and instrumentation. Rack and bench removal from the cabin allowed for the addition of seats. The additions and removals changed the LCG to 10.55 feet from the transom-keel intersection (Murphy & Planchak, 2015).

Beginning in the summer of 2015, Old Dominion University students and NEMSI faculty advisors conducted an initial investigation to consider the use of full-scale vertical acceleration data as forced input for direct transient analysis of a high speed craft, using commercial finite element analysis software (Trenor, Sanders, Johnson, Michaeli, & Hou, 2015). Although

completion of modal analysis was not one of the main objectives of this current study, the method utilized and associated results are discussed to provide total transparency into the research effort as a whole. Modal analysis of the finite element model was performed for three boundary conditions. The boundary conditions included an unconstrained condition, 1 Hertz springs, and 2 Hertz springs. The 1 Hertz spring constraints and 2 Hertz spring constraints were applied to the hull of the finite element model and allowed for the approximation of percent modal mass participation at various frequencies. The modes of interest included the primary hull bending mode and main deck flexural modes.

Research at Old Dominion University commenced with the investigation into modal analysis data. As previously mentioned, NSWCCD Code 661 completed a modal analysis through the use of NEiNASTRAN. At Old Dominion University, MSC NASTRAN was used to complete a modal analysis of the finite element model developed by NSWCCD Code 661. The differences in results were then investigated. Sample results from the three boundary conditions investigated are listed in Table 2.

Table 2. MSC Nastran Modal Sample Results (Trenor et al., 2015)

No Boundary Conditions			1 Hz Springs Boundary Conditions			2 Hz Springs Boundary Conditions		
Mode	f (Hz)	% Errror	Mode	f (Hz)	% Errror	Mode	f (Hz)	% Errror
11	8.1375	0.76	7	8.1308	0.84	7	8.1309	0.84
17	12.657	0.45	14	12.64	0.32	14	12.65	0.4
12	8.8144	0.96	9	9.9449	0.48	9	10.066	0.48

Modal analysis of the RIB was achieved through the creation and application of 1 hertz and 2 hertz springs upon the finite element model. Modal analysis results were compared against data provided in NSWCCD Code 60's report for accuracy purposes. Comparison of the modal

analysis completed in MSC NASTRAN to that conducted in NEiNASTRAN allowed for the adjustment of the model to a more accurate spring constant. During this investigation, 200 modes were analyzed and averaged for each condition analyzed. The MSC NASTRAN modal analysis, for the entire boat, yielded an averaged error of 1.16%, 1.20%, and 1.14% for the free boundary, 1 Hertz springs, and 2 Hertz springs boundary conditions respectively (Trenor et al., 2015). The maximum error realized was that of mode 22 of the free boundary condition model, at 2.97% (Trenor et al., 2015).

2.2.2 Acceleration Data

In 2014, NSWCCD Code 835 completed sea trials on an 11-meter cabin RIB in an effort to investigate wave impact phenomena (Murphy & Planchak, 2015). During sea trials, investigators collected acceleration data through multiple sea states. The specific sea states are shown in Table 3 below.

Table 3. Completed Seakeeping Runs

Date	Target Seakeeping Run	Average Craft Speed (kn)	Significant Wave Height (ft)	Average Wave Period (s)
Feb 12, 2014	2014Feb12 Head Sea Max Safe Speed	25.7	3.9	5.6
Feb 12, 2014	2014Feb12 Head Sea 15kt Avg Speed	18.9	3.9	5.6
Feb 21, 2014	2014Feb21 Head Sea 15kt Avg Speed	14.9	3.9	5.7
Feb 10, 2014	2014Feb10 Head Sea Max Safe Speed	20.2	4.6	5.2
Mar 11, 2014	2014Mar11 Head Sea 20kt Avg Speed	20.5	2.2	7.2
Mar 12, 2014	2014Mar12 Head Sea 20kt Avg Speed	20.3	3.4	6.4
Feb 13, 2014	2014Feb13 Head Sea Max Safe Speed	19.0	5.0	6.2
Mar 11, 2014	2014Mar11 Head Sea Max Safe Speed	35.8	2.3	7.5
Mar 12, 2014	2014Mar12 Head Sea 30kt Avg Speed	30.4	3.4	6.4

Column 1 provides the date that the data was collected. Column 2 details the name under which the dataset was saved. Column 3 is the average speed of the vessel while data was

collected. Column 4 is the significant wave height, which “is the average of the one-third highest waves as measured from crest to trough during a wave measurement period” (Murphy & Planchak, 2015). Column 5 is the average period of the waves while data was collected.

The data collected was categorized into three envelopes depending upon head-sea runs condition. The top three runs listed in Table 3 are where the significant wave-heights were about the same over three different average craft speeds and make up the Constant Wave Height Envelope. The middle three runs are where the average craft speed was approximately the same over three different wave-heights and make up the Constant Speed Envelope. The last three runs are where the RIB was at or near the maximum safe speed for the boat operator and makes up the Maximum Safe Speed Envelope. In-depth details of the data collection effort are presented in (Murphy & Planchak, 2015).

2.2.3 StandardG Algorithm

Wave impact response is a combination of rigid body motion, structural flexure, and vibration, as shown in Figure 1 (Riley & Coats, 2013). In an effort to retain and sort the accelerations that are not associated with local flexible body vibration, the StandardG algorithm was utilized.

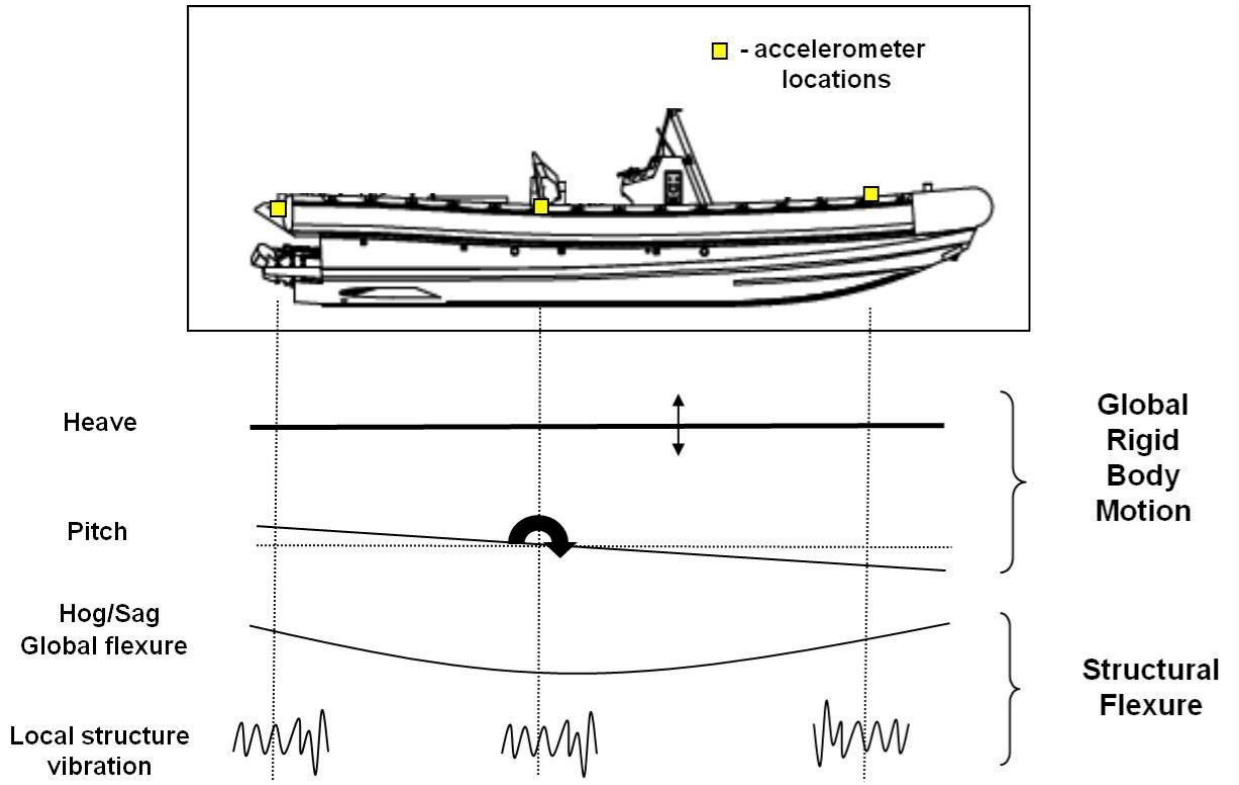

Figure 1. Rigid Body Motion and Structural Flexure (Riley & Coats, 2013)

The StandardG algorithm is a "standardized algorithm for extracting rigid body accelerations from acceleration data" (Riley & Coats, 2013). Also known as the Peak Identification Algorithm, it is one of the analysis methods employed by NSWCCD DN. "The peak-finding algorithm compares each point, ai, with a window of points between ai – time and ai + time. A value is considered a peak if it exceeds the amplitude threshold and is greater than the time threshold on either side of the point under evaluation. In short, the algorithm verifies that each peak is greater than the selected amplitude and only one peak occurs over the time threshold" (Murphy & Planchak, 2015). Figure 2 depicts the peak selection method performed on raw accelerometer data from sea trials.

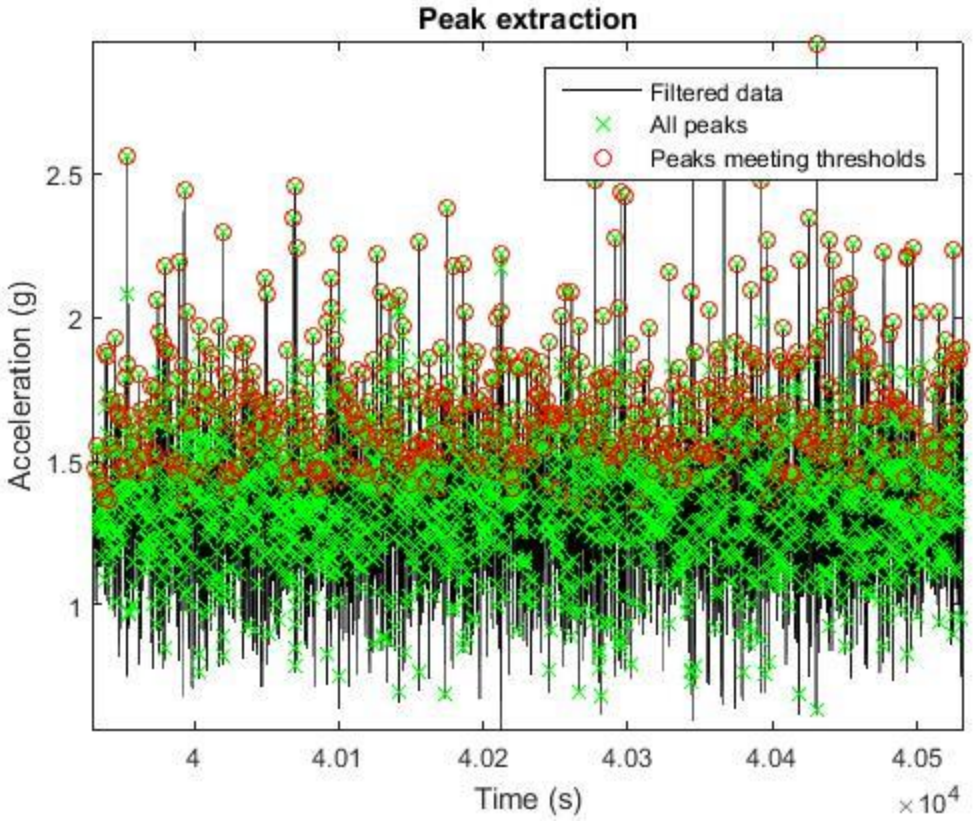

Figure 2. Peak Extraction Plot from Accelerometer 11Z

The StandardG algorithm processed all of the filtered acceleration data presented in this study. Although other software may be used to run the algorithm, MATLAB was utilized throughout the entire study. When running the program in MATLAB, the user is able to load acceleration data in the form of a Text File (.txt). Then, A Fast Fourier Transform (FFT) algorithm is used to plot amplitude versus frequency of the loaded data. A fourth order Butterworth low pass filter is then used to filter the loaded data to a user defined cutoff frequency.

In order to reduce the amount of Nastran computations, the MATLAB file provided by NSWCCD Combatant craft was modified. However, the core operation of the StandardG algorithm was not altered. Further details of the modification are discussed in Chapter 3.

CHAPTER 3

3. DYNAMIC RESPONSE MODELING OF A HIGH SPEED PLANING CRAFT WITH ENFORCED ACCELERATION

This chapter is dedicated to the discussion of dynamic response modeling and the information necessary for its implementation.

3.1 Equation of Motion under Base Excitation

The derivation of equations associated with base excitation are presented hereafter. The theoretical formulations are the basic foundation for the operation of software used to complete enforced acceleration. The equation of motion is derived based upon Differential-Algebra Equation (DAE) point of view.

The equation of motion of a free flexible structure under the given loading $\boldsymbol{p}(t)$ can be described as

$$M\ddot{\boldsymbol{x}} + C\dot{\boldsymbol{x}} + K\boldsymbol{x} = \boldsymbol{p}(t) \qquad (1)$$

where M, C and K are the mass, damping and stiffness matrices and $\boldsymbol{p}(t)$ and $\boldsymbol{x}(t)$ are the force and the displacement vectors. The displacement vector $\boldsymbol{x}(t)$ is unknown. The above equation maybe simplified as

$$M\ddot{\boldsymbol{x}} = \boldsymbol{f}(t, \boldsymbol{x}, \dot{\boldsymbol{x}}) \equiv \boldsymbol{p}(t) - C\dot{\boldsymbol{x}} - K\boldsymbol{x}$$

In the case of enforced motion, a given set of degrees of freedom of the system are subjected to enforced acceleration, which can be viewed as constraints imposed upon Eq. (1). That is,

$$M\ddot{\boldsymbol{x}} = \boldsymbol{f}(t, \boldsymbol{x}, \dot{\boldsymbol{x}}) \text{ subjected to } \ddot{\boldsymbol{x}}_{\boldsymbol{B}} \equiv \boldsymbol{a}(t) \quad (2)$$

where the displacement vector is divided into two parts, prescribed or free, $\boldsymbol{x}^{\boldsymbol{T}} = (\boldsymbol{x}_{\boldsymbol{I}} \quad \boldsymbol{x}_{\boldsymbol{B}})$ of which the accelerations of degrees of freedom at $\boldsymbol{x}_B$ are prescribed by given values, $\boldsymbol{a}(t)$. That is, the system equation is subjected to the constraint,

$$\ddot{\boldsymbol{x}}_B = \boldsymbol{a}(t) \qquad (3)$$

This constraint is integrated which leads to the velocity and the position constrains $\dot{\boldsymbol{x}}_{\boldsymbol{b}} \equiv \boldsymbol{a}t + \dot{\boldsymbol{u}}_0$ and $\boldsymbol{x}_{\boldsymbol{b}} \equiv \frac{1}{2}\boldsymbol{a}t^2 + \dot{\boldsymbol{u}}_0 t + \boldsymbol{u}_0$, with given initial velocity and position, $\boldsymbol{u}_0$ and $\dot{\boldsymbol{u}}_0$. As the displacement constraint is holonomic, Eq. (2) can be augmented by introducing the Lagrange multipliers λ as

$$\begin{bmatrix} M_{II} & M_{IB} & 0 \\ M_{BI} & M_{BB} & I \\ 0 & I & 0 \end{bmatrix} \begin{Bmatrix} \ddot{\boldsymbol{x}}_{\boldsymbol{I}} \\ \ddot{\boldsymbol{x}}_{\boldsymbol{B}} \\ \boldsymbol{\lambda} \end{Bmatrix} = \begin{Bmatrix} \boldsymbol{f}_{\boldsymbol{I}}(t, \boldsymbol{x}_I, \dot{\boldsymbol{x}}_I, \boldsymbol{x}_B, \dot{\boldsymbol{x}}_B) \\ \boldsymbol{f}_{\boldsymbol{B}}(t, \boldsymbol{x}_I, \dot{\boldsymbol{x}}_I, \boldsymbol{x}_B, \dot{\boldsymbol{x}}_B) \\ \boldsymbol{a}(t) \end{Bmatrix} \quad (4)$$

subject to two hidden constraints,

$$\left.\begin{aligned} \dot{\boldsymbol{x}}_{\boldsymbol{B}} &\equiv \boldsymbol{a}t + \dot{\boldsymbol{u}}_0 \\ \boldsymbol{x}_{\boldsymbol{B}} &\equiv \frac{1}{2}\boldsymbol{a}t^2 + \dot{\boldsymbol{u}}_0 t + \boldsymbol{u}_0 \end{aligned}\right\} \quad (5)$$

The most convenient approach to solve the DAE system, Eqs. (4) and (5), is by direct substitution. The resultant equations become

$$\begin{bmatrix} M_{II} & 0 \\ M_{BI} & I \end{bmatrix} \begin{Bmatrix} \ddot{\boldsymbol{x}}_I \\ \boldsymbol{\lambda} \end{Bmatrix} = \begin{Bmatrix} \boldsymbol{f}_I - M_{IB}\boldsymbol{a} \\ \boldsymbol{f}_{\boldsymbol{B}} - M_{BB}\boldsymbol{a} \end{Bmatrix} \quad (6)$$

The first row of Eq. (6) is a typical ODE which can be solved with help of Eq. (3) as

$$M_{II}\ddot{\boldsymbol{x}}_{\boldsymbol{I}} = \boldsymbol{f}_{\boldsymbol{I}}(t, \boldsymbol{x}_I, \dot{\boldsymbol{x}}_I, \boldsymbol{x}_B, \dot{\boldsymbol{x}}_B) - M_{IB}\ddot{\boldsymbol{x}}_B = \boldsymbol{f}_{\boldsymbol{I}}(t, \boldsymbol{x}_I, \dot{\boldsymbol{x}}_I, \boldsymbol{u}_0, \dot{\boldsymbol{u}}_0, \boldsymbol{a}) - M_{IB}\boldsymbol{a}$$

which leads to the solutions of $\boldsymbol{x}_{\boldsymbol{I}}(t)$ and $\dot{\boldsymbol{x}}_{\boldsymbol{I}}(t)$. The latter can be used to find the Lagrange multiplier in the second row of Eq. (6) as

$$\boldsymbol{\lambda} = \boldsymbol{f}_{\boldsymbol{B}}(t, \boldsymbol{x}_I, \dot{\boldsymbol{x}}_I, \boldsymbol{x}_B, \dot{\boldsymbol{x}}_B) - M_{BI}\ddot{\boldsymbol{x}}_I - M_{BB}\ddot{\boldsymbol{x}}_B = \boldsymbol{f}_{\boldsymbol{B}}(t, \boldsymbol{x}_I, \dot{\boldsymbol{x}}_I, \boldsymbol{u}_0, \dot{\boldsymbol{u}}_0, \boldsymbol{a}) - M_{BI}\ddot{\boldsymbol{x}}_I - M_{BB}\boldsymbol{a}$$

or more specifically,

$$\boldsymbol{\lambda} = \boldsymbol{f}_{\boldsymbol{B}}(t, \boldsymbol{x}_I, \dot{\boldsymbol{x}}_I, \boldsymbol{u}_0, \dot{\boldsymbol{u}}_0, \boldsymbol{a}) - M_{BI}M_{II}^{-1}\boldsymbol{f}_I + \left(M_{BI}M_{II}^{-1}M_{IB} - M_{BB}\right)\boldsymbol{a}$$

It should be noted that Eq. (2) can be extended to cases with enforced displacements and velocities in which the acceleration constraint is obtained through differentiation.

3.2 PATRAN and NASTRAN Solution Procedure for Enforced Acceleration

Filtered Raw accelerometer data from sea trials was initially used as input for all dynamic response modeling. In order to allow for the import of acceleration data into PATRAN, each accelerometer dataset was saved as CSV files. Accelerometer data was assigned to finite element model nodes with the approximate locations of the accelerometer used during sea trials. For comparison purposes, specific accelerometers on the RIB pilot cabin were not enforced. Within PATRAN, a transient response solution was requested. From PATRAN, a BDF file is generated with the prescribed enforced data. The BDF file is then imported into NASTRAN for computation of the requested transient response. From NASTRAN, an f06 file is generated with the requested data output. Detailed instructions are provided in Appendix A. Figure 3 displays the exact MSC NASTRAN commands and functions utilized to create the final load used during simulation.

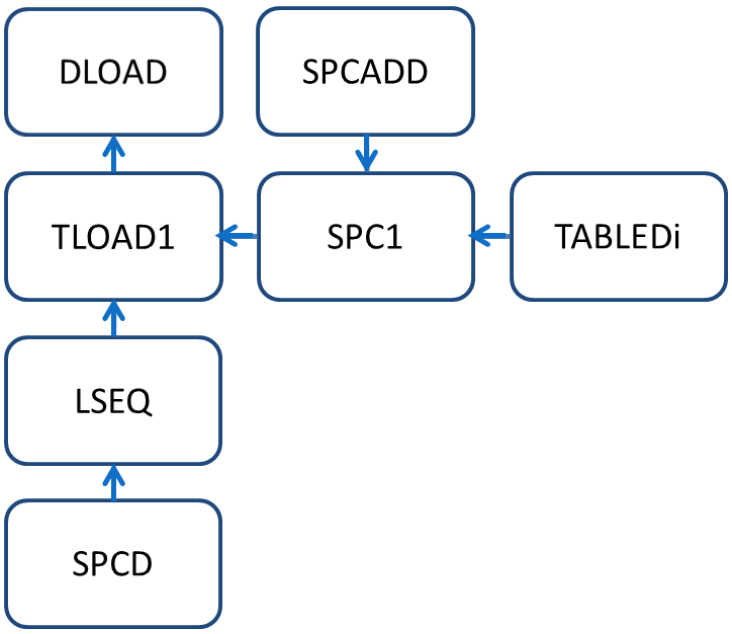

Figure 3. MSC NASTRAN Acceleration Input Flowchart

The NASTRAN solution procedure for this research centered on the SPC1 and TLOAD1 arguments. These commands allowed for direct input of acceleration data from the selected accelerometers into the NASTRAN solution.

Acceleration data was input as TABLEDi data values and referenced into the SPC1 arguments defined by SPCADD. On the full boat analysis, there were 11 SPC1(s) that corresponded to 11 of the accelerometer locations. The isolated cabin analysis used 7 input acceleration locations. The acceleration data for one slam event from each accelerometer was input at the model nodal location that corresponded to the physical location on the real-world boat.

The TLOAD1 arguments combined the SPC1(s) and the enforced motion SPCD's. The SPCD(s) were located at the same nodes as the SPC1(s). These TLOAD1 commands were incorporated into the single DLOAD argument along with their respective load scale factors, and the solution process was then started.

3.3 Full Boat Validation

In order to be able to justify the use of stress and displacement results from the integration of the developed finite element model and sea trial data, it was necessary to first show that the integration of the two data types approximated real dynamic conditions. A summary of the method used during the full boat validation is provided in Figure 4.

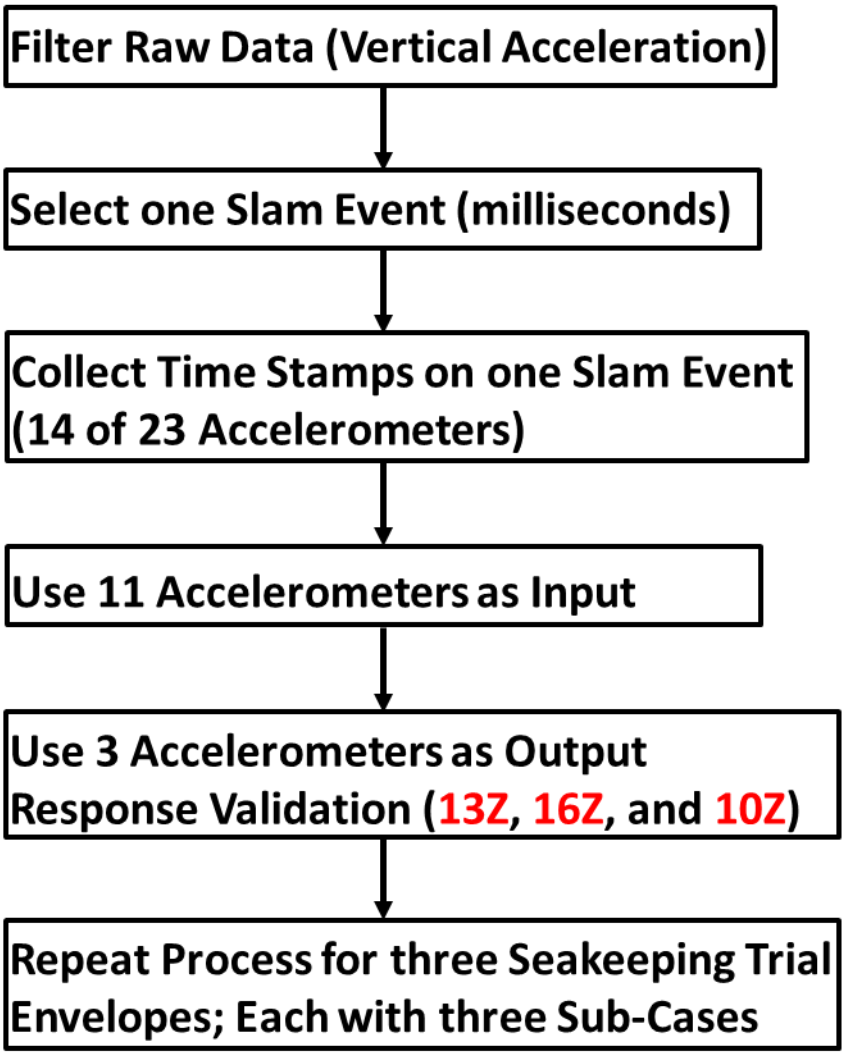

Figure 4. Full Boat Validation Flowchart

The validation process began with analysis of the data collected during sea trials. Figure 5 depicts a graphical representation of the raw experimental data for one subcase. In order to extract the full boat acceleration without the noise from local flexible body vibration, all of the acceleration data was filtered at 10 Hertz. The selection of the cutoff frequency was selected by analysis of the spectrum plot created through the StandardG algorithm. As shown in Figure 6, the amplitude greatly diminishes after 10 Hertz.

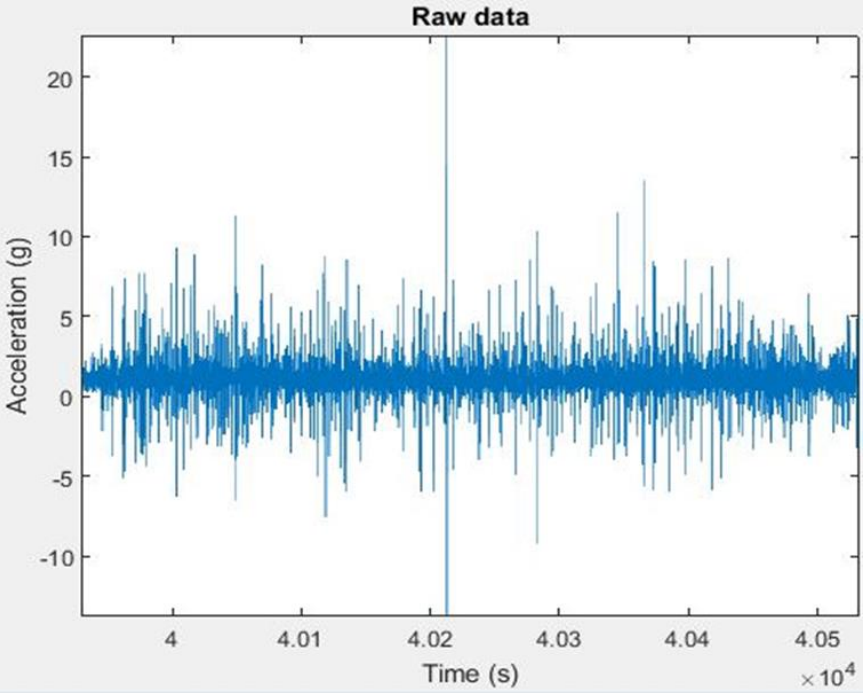

Figure 5. Subcase 3 of Constant Speed Envelope: Accelerometer 1Z Raw Data Plot

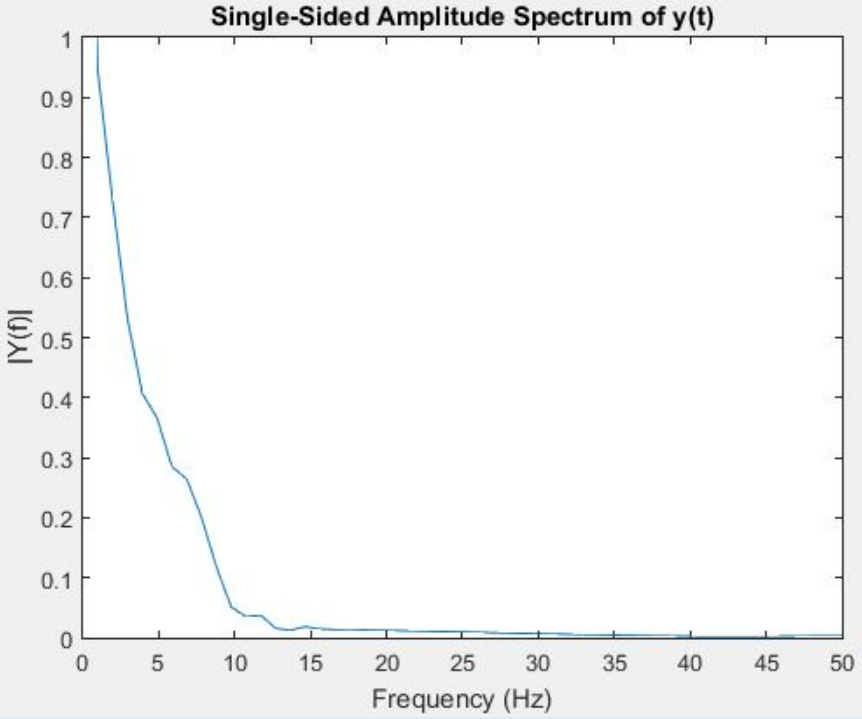

Figure 6. Subcase 3 of Constant Speed Envelope: 1Z Full Boat Spectrum Plot

In order to reduce simulation time, the validation investigation focused upon a specific impact event during the experimental trial. Selection of a specific event within the sea trial data was completed through the use of the StandardG algorithm. Raw data from accelerometer 11Z, located near the longitudinal center of gravity, was used as a gauge for the sea trial event of interest. The peak acceleration from accelerometer 11Z marked the wave impact event to be studied. In addition to providing the peak acceleration, the StandardG algorithm also detailed the time at which the peak acceleration occurred. Following the location of the single highest acceleration near the LCG, modification of the StandardG algorithm was completed in order to collect data points before and after the time of the peak acceleration for a total of 2000 points over a 1 second event. Of the 2000 points within the 1-second interval 500 data points were used to represent the event by filtering for every fourth point. The selection of a 1-second interval was completed for each of the nine subcases.

The process reduces MSC NASTRAN computation. Filtered and comparison plots of the data are provided in Appendix B.

With filtered accelerometer data available, the next step was to find the locations that best estimated the actual placement of the accelerometers during sea trials. Although the finite element model was highly detailed, the RIB and finite element model do not share all of the same structural components. Due to the differences in the experimental vessel and modeled vessel, only eleven sets of the available accelerometer data could be used as inputs during enforced excitation. The eleven accelerometers include 1Z, 2Z, 3Z, 4Z, 6Z, 7Z, 8Z, 9Z, 11Z, 17Z, and 21Z. The locations of said accelerometers are presented in Figures 7 and 8. The current study made use of the accelerometers oriented in the vertical direction, which is normal to the deck. In Figure 7, the vertical accelerometers are designated with a red arrow. In Figure 8, the

vertical accelerometers are designated with a red dot. The physical locations of the vertical accelerometers on the 11m RIB used during sea trials are specified in Table 4 below.

Table 4. Accelerometer Locations on 11-meter Cabin RIB

Accelerometer	Location Description
1Z	Keel, forward of deckhouse, bolted to centerline longitudinal structural support
2Z	Forward centerline engine box, bolted on accelerometer block
3Z	Transom-keel, in bilge, bolted to centerline structural support
4Z	Transom, deck height, epoxied to 15-degree resin wedge
6Z	Keel, bow forward-most compartment, mounted in molded resin epoxy
7Z	Deck, forward of cabin, centerline (longitudinally between 1Z and 6Z) middle of deck plate
8Z	Deck, centerline at base of cabin, forward bulkhead
9Z	Deck, port side at base of cabin, forward bulkhead
10Z	Deck, centerline, inside cabin on deck plate
11Z	Main deck centerline at base of cabin door, installed on battery bank in IMU box at the LCG
13Z	Console, centerline, inside cabin at coxswain controls
16Z	Cabin top, centerline at LCG
17Z	Port shock mitigation seat, deck input, outboard
21Z	Starboard fixed seat, deck input, outboard

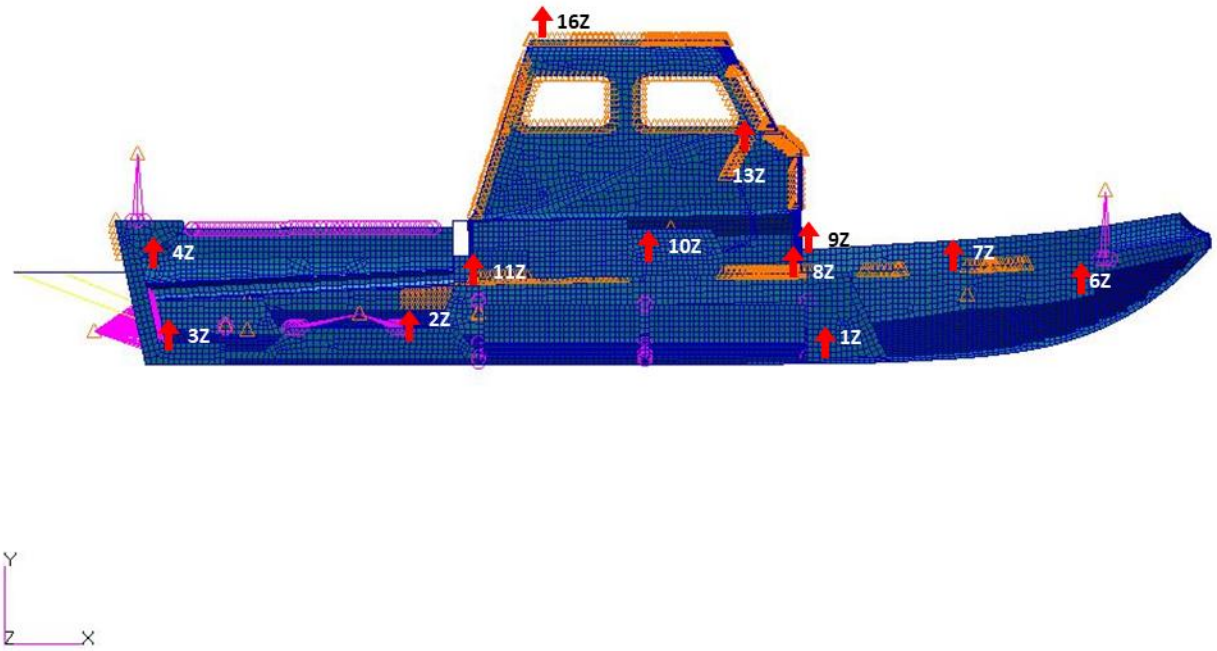

Figure 7. Side-View of 11-meter Cabin RIB Model with Accelerometer Locations

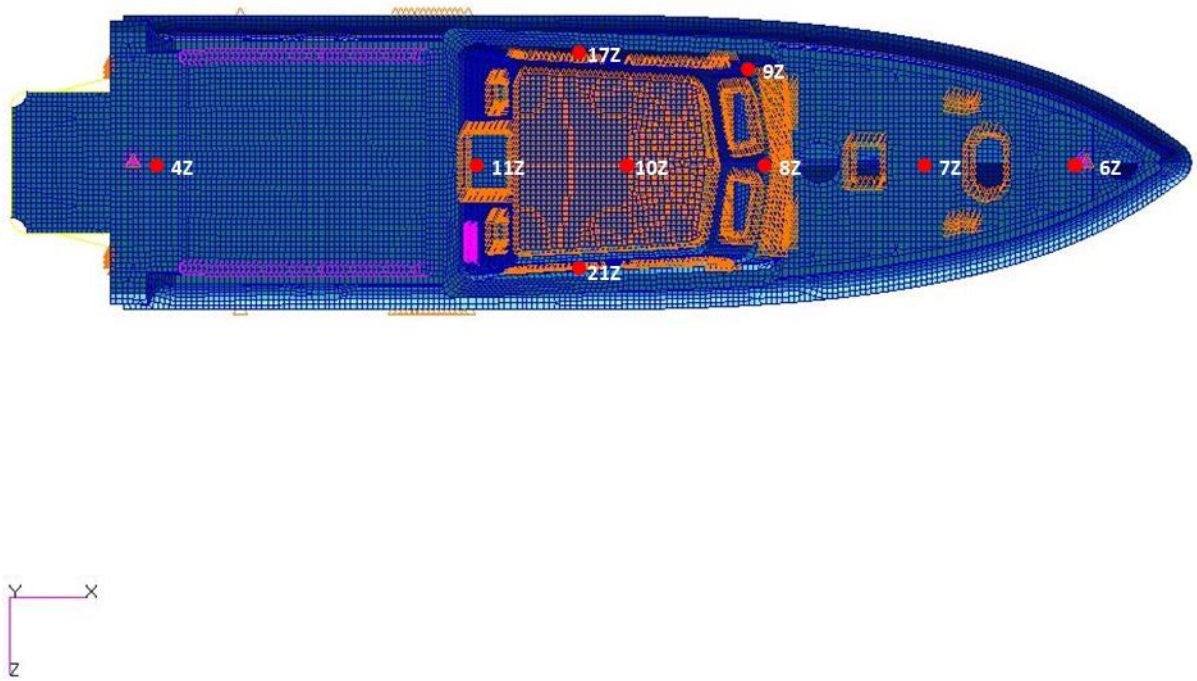

Figure 8. Top-View of 11-meter Cabin RIB Model with Accelerometer Locations

In order to simulate the dynamic effects, the time-dependent accelerations were input through PATRAN and solved by MSC NASTRAN, a method that was previously discussed in section 3.2 and further divulged in Appendix A. During direct transient analysis of the model, numerical output of dynamic responses at selected nodes, 10Z, 13Z, and 16Z filtered at 10 hertz, were compared against collected acceleration data provided by NSWCCD Code 80's sea trials. When implementing full-boat enforced acceleration, accelerometers 1Z, 2Z, 3Z, 4Z, 6Z, 7Z, 8Z, 9Z, 11Z, 17Z, and 21Z were input at nodes 9131, 38278, 47452, 50220, 933, 5096, 10611, 11521, 29178, 29640, and 29446 respectively.

The above approach was taken for a total of three sea-keeping trial envelopes, each with three sub-cases, which are detailed in Table 3. Graphs of the filtered raw data and filtered MSC NASTRAN output for the three sea-keeping trial envelopes are shown below with their respective changes in standard deviation and root mean square mean deviation values. Microsoft Excel was used for the calculations of standard deviation and root-mean-square deviation. With respect to the investigation conducted, the calculations included:

Letting the error be defined for every sampling time for a total of 500 sampled data in one second of an impact event,

$$\varepsilon_i \equiv abs\left(a_i^{\exp} - a_i^{sim}\right) \text{ For } i = 1 \text{ to } 500$$

where $a_i^{\exp}$ is obtained from the filtered raw data collected from an accelerometer, while a_i^{sim} is from the filtered MSC NASTRAN simulation result.

The mean of the error is obtained for n samples by,

$$\mu = \frac{\sum_i^n \varepsilon_i}{n}$$

and its associated variance is obtained by,

$$\sigma^2 = \frac{\sum_{i}^{n} (\varepsilon_i - \mu)^2}{n}$$

with the square root of variance providing the standard deviation. The root-mean-square deviation is obtained by,

$$RMS = \sqrt{\frac{\sum_{i=1}^{n} \varepsilon_i^2}{n}}$$

The results and process are further summarized in the tables and figures displayed below.

The Constant Speed Envelope data, used to generate Figures 9(a), 9(b), and 9(c), was collected on February 10, 2014, March 11, 2014, and March 12, 2014 respectively, as listed in Table 3. The data of concern is grouped into three subcases. Subcase 1 was collected at average craft speed of 20.2 knots, significant wave height of 4.6 feet, average wave period of 5.2 seconds, and is depicted in Figure 9(a). Subcase 2 was collected at average craft speed of 20.5 knots, significant wave height of 2.2 feet, average wave period of 7.2 seconds, and is depicted in Figure 9(b). Subcase 3 was collected at average craft speed of 20.3 knots, significant wave height of 3.4 feet, average wave period of 7.2 seconds, and is depicted in Figure 9(c). Comparisons of the filtered MSC NASTRAN output to that of the full boat filtered raw data are shown in Figure 9.

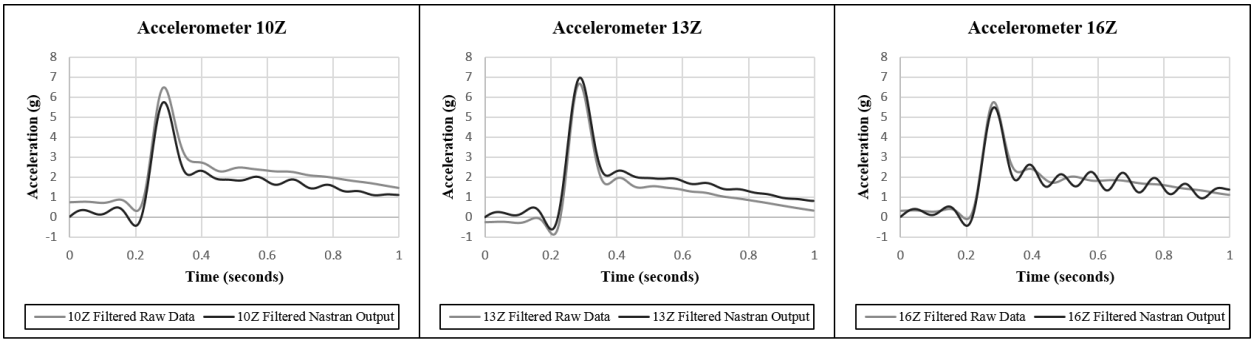

(a) Filtered Subcase 1 of Constant Speed Envelope. Average Craft Speed 20.2 knots. Significant Wave Height 4.6 feet. Average Wave Period 5.2 seconds.

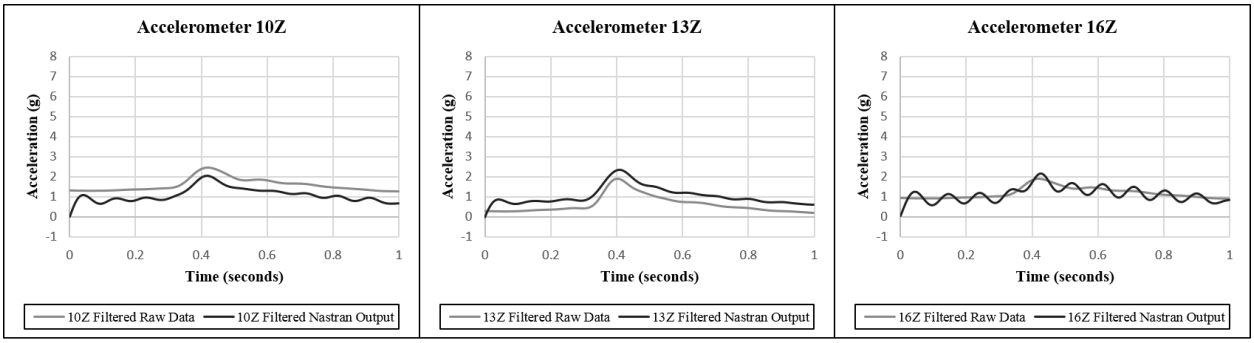

(b) Filtered Subcase 2 of Constant Speed Envelope. Average Craft Speed 20.5 knots. Significant Wave Height 2.2 feet. Average Wave Period 7.2 seconds.

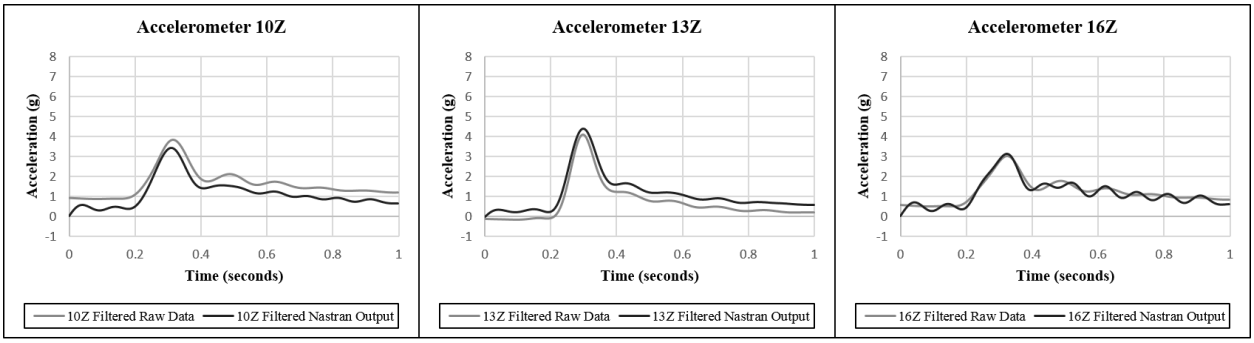

(c) Filtered Subcase 3 of Constant Speed Envelope. Average Craft Speed 20.3 knots. Significant Wave Height 3.4 feet. Average Wave Period 6.4 seconds.

Figure 9. Filtered Constant Speed Envelope

The Constant Wave Height Envelope data used to generate Figures 10(a), 10(b), and 10(c) was collected on February 12, 2014, February 12, 2014, and February 21, 2014 respectively, as listed in Table 3. The data of concern is grouped into three subcases. Subcase 1 was collected at average craft speed of 25.7 knots, significant wave height of 3.9 feet, average wave period of 5.6 seconds, and is depicted in Figure 10(a). Subcase 2 was collected at average craft speed of 18.9 knots, significant wave height of 3.9 feet, average wave period of 5.6 seconds, and is depicted in Figure 10(b). Subcase 3 was collected at average craft speed of 14.9 knots, significant wave height of 3.9 feet, average wave period of 5.7 seconds, and is depicted in Figure 10(c). Comparisons of the filtered MSC NASTRAN output to that of the full boat filtered raw data are shown in Figure 10.

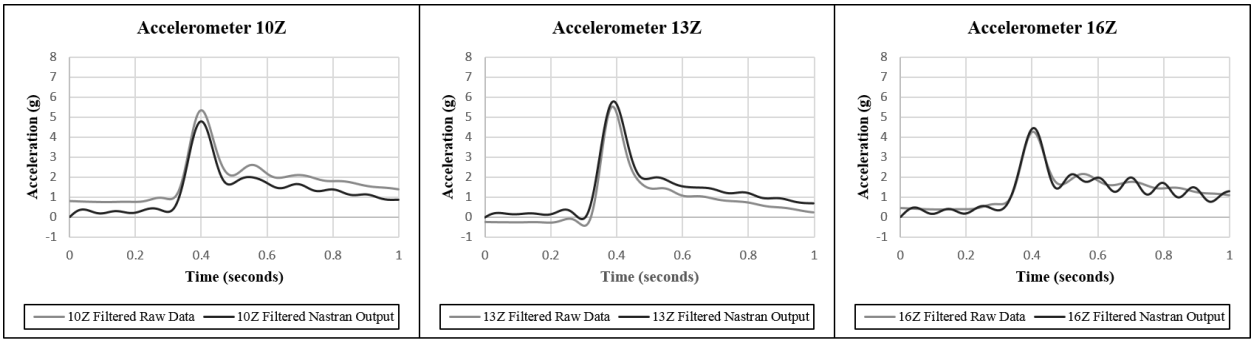

(a) Filtered Subcase 1 of Constant Wave Height Envelope. Average Craft Speed 25.7 knots. Significant Wave Height 3.9 feet. Average Wave Period 5.6 seconds.

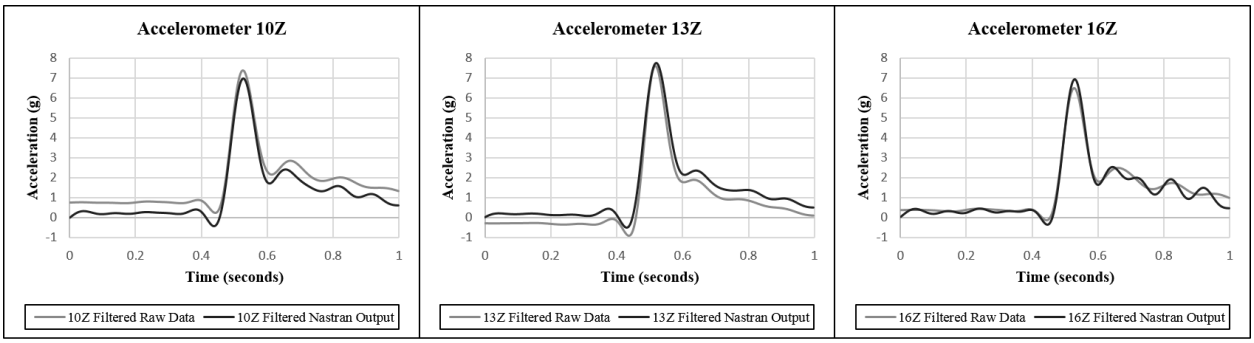

(b) Filtered Subcase 2 of Constant Wave Height Envelope. Average Craft Speed 18.9 knots. Significant Wave Height 3.9 feet. Average Wave Period 5.6 seconds.

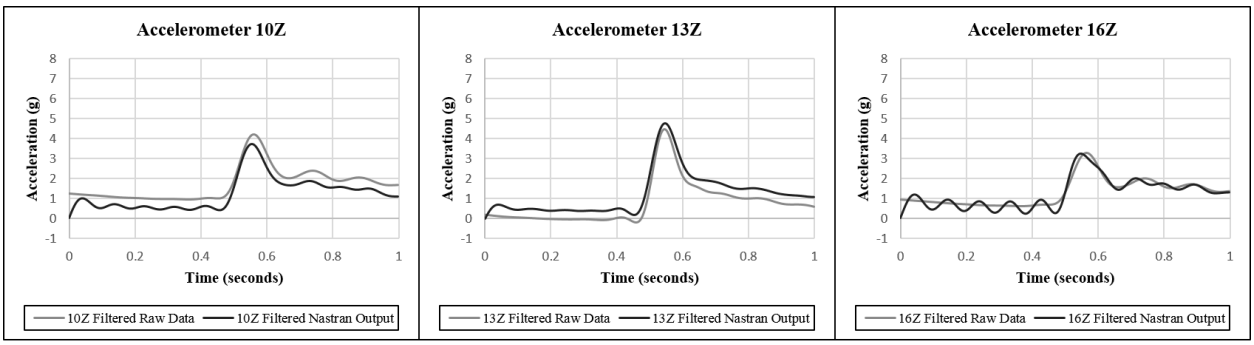

(c) Filtered Subcase 3 of Constant Wave Height Envelope. Average Craft Speed 14.9 knots. Significant Wave Height 3.9 feet. Average Wave Period 5.7 seconds.

Figure 10. Filtered Constant Wave Height Envelope

The Maximum Safe Speed Envelope data used to generate Figures 11(a), 11(b), and 11(c) was collected on February 13, 2014, March 11, 2014, and March 21, 2014 respectively, as listed in Table 3. The data of concern is grouped into three subcases. Subcase 1 was collected at average craft speed of 19.0 knots, significant wave height of 5.0 feet, average wave period of 6.2 seconds, and is depicted in Figure 11(a). Subcase 2 was collected at average craft speed of 35.8 knots, significant wave height of 2.3 feet, average wave period of 7.5 seconds, and is depicted in Figure 11(b). Subcase 3 was collected at average craft speed of 30.4 knots, significant wave height of 3.4 feet, average wave period of 6.4 seconds, and is depicted in Figure 11(c). Comparisons of the filtered MSC NASTRAN output to that of the full boat filtered raw data are shown in Figure 11.

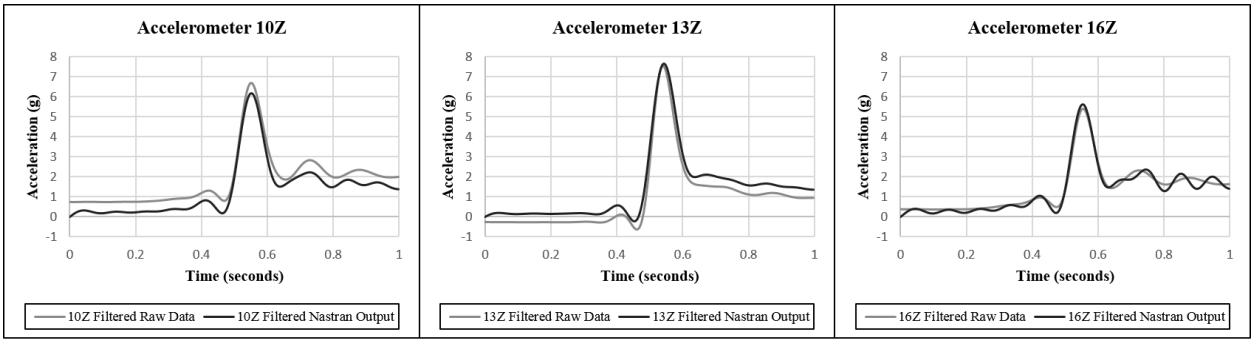

(a) Filtered Subcase 1 of Maximum Safe Speed Envelope. Average Craft Speed 19.0 knots. Significant Wave Height 5.0 feet. Average Wave Period 6.2 seconds.

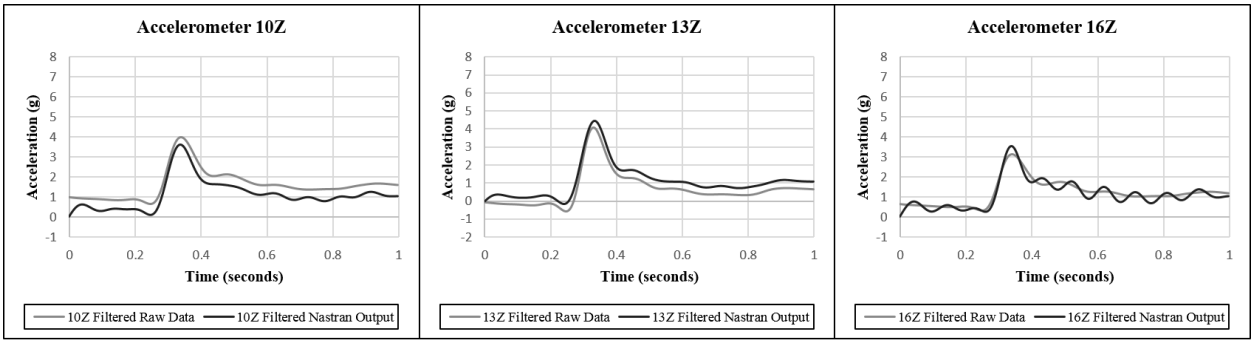

(b) Filtered Subcase 2 of Maximum Safe Speed Envelope. Average Craft Speed 35.8 knots. Significant Wave Height 2.3 feet. Average Wave Period 7.5 seconds.

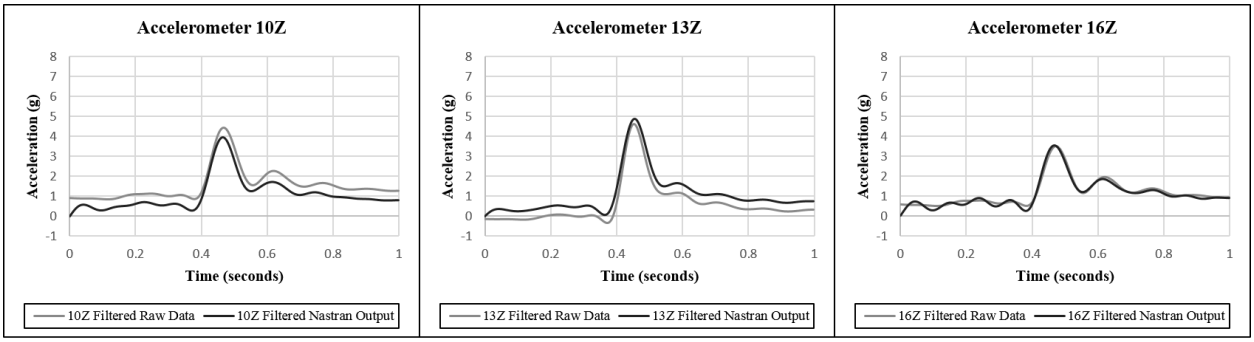

(c) Filtered Subcase 3 of Maximum Safe Speed Envelope. Average Craft Speed 30.4 knots. Significant Wave Height 3.4 feet. Average Wave Period 6.4 seconds.

Figure 11. Filtered Maximum Safe Speed Envelope

The investigation found that enforced acceleration upon the finite element model was able to yield results that correlated with the information obtained during sea trial data collection. The statement of correlation between the two sets of data is based upon graphical and numerical evidence. The graphical evidence is represented by time-dependent acceleration curves, while the numerical evidence included both the calculation of root mean square deviation and standard deviation. A compilation of the data calculations for the three envelopes is shown is Table 5.

Table 5. Envelope Deviation (g's): 11 Accelerometers as Input

ENVELOPE	SUBCASE	10Z RMSD	13Z RMSD	16Z RMSD	10Z STDEV	13Z STDEV	16Z STDEV
CONSTANT SPEED ENVELOPE	SUBCASE 1	0.5506	0.4591	0.2606	0.0153	0.0069	0.0178
CONSTANT SPEED ENVELOPE	SUBCASE 2	0.4965	0.4416	0.2239	0.0103	0.0032	0.0134
CONSTANT SPEED ENVELOPE	SUBCASE 3	0.4863	0.4428	0.1725	0.0094	0.0036	0.0081
CONSTANT WAVE HEIGHT ENVELOPE	SUBCASE 1	0.5199	0.4763	0.2237	0.0135	0.0171	0.0206
CONSTANT WAVE HEIGHT ENVELOPE	SUBCASE 2	0.5224	0.4708	0.2046	0.0066	0.0092	0.0130
CONSTANT WAVE HEIGHT ENVELOPE	SUBCASE 3	0.4950	0.4608	0.2137	0.0149	0.0068	0.0167
MAXIMUM SAFE SPEED ENVELOPE	SUBCASE 1	0.5153	0.4869	0.1769	0.0146	0.0161	0.0112
MAXIMUM SAFE SPEED ENVELOPE	SUBCASE 2	0.4957	0.4428	0.2113	0.0071	0.0042	0.0126
MAXIMUM SAFE SPEED ENVELOPE	SUBCASE 3	0.4861	0.4477	0.1258	0.0090	0.0062	0.0059

The range of filtered root mean square deviation included a minimum of 0.1258 g's, found through the Maximum Safe Speed Envelope, and a maximum of 0.5506 g's, found through the Constant Speed Envelope. The range of standard deviation included a minimum of 0.0032 g's, found through the Constant Speed Envelope, and a maximum of 0.0206, found through the Constant Wave Height Envelope. Overall, finite element model validation through enforced excitation by point accelerations and comparison to sea trial data was found to be effective.

In this study, Constant Speed Envelope was the first envelope to be analyzed. Subcase 3 of Constant Speed Envelope was found to correlate the best with filtered raw data, as supported by the calculations of root mean square deviation and standard deviation. In order to remain

consistent, Subcase 3 of Constant Speed Envelope was used for completion of all subsequent investigations. The use of a single subcase was justified by the fact that the application of enforced acceleration, documentation of procedure, and analysis of effects were the core interests. The same procedures to be discussed can be completed on any of the nine subcases.

CHAPTER 4

4. ENGINEERING APPLICATIONS

This chapter is dedicated to the discussion of the effects of the number and placement of accelerometers.

4.1 Sensitivity Study

During the accelerometer sensitivity study of the model, dynamic responses at selected pilot cabin nodes were compared against collected acceleration data provided by NSWCCD Code 80's sea trials, following the removal of selected accelerometer sets. The sensitivity study was conducted using full-boat enforced acceleration. Therefore, node and accelerometer listing remained consistent with the finite element model validation effort previously discussed in Chapter 3.

In order to investigate the sensitivity, and or response, of the finite element model to reduction in the quantity of acceleration sensors and locate the most vital accelerometers, accelerometer outputs from 10Z, 13Z, and 16Z were used to gauge response quality. Due to the overall correlation found when conducting the finite element model validation investigation of Constant Speed Envelope at 20.3 knots and significant wave height of 3.4 feet, its data was used as a model dataset during completion of the sensitivity study.

The study commenced through the removal of any nodes not located along the RIB's longitudinal center of gravity. This was accomplished by removing data associated with accelerometer 17Z and accelerometer 9Z, on the port side, and accelerometer 21Z on the starboard side to complete the first case study. From there, the effect of a single port or starboard input was investigated. This was accomplished by (1) removing data associated with accelerometer 17Z and accelerometer 9Z in the second case study, (2) removing data associated

with accelerometer 17Z and accelerometer 21Z in the third case study, and (3) removing data associated with accelerometer 21Z and accelerometer 9Z in the fourth case study.

The final three cases investigated a symmetric input environment. In order to investigate a symmetric input scenario, (1) accelerometer 9Z was removed in the fifth case study, (2) accelerometer 9Z and accelerometer 4Z were removed in the sixth case study, and (3) accelerometer 8Z and accelerometer 9Z were removed in the seventh case study. Accelerometers were removed from the FE model through node deletion within PATRAN. The decision of accelerometer deletion and reapplication during the sensitivity study was wholly based upon changes in the root mean square deviation and standard deviation values. The procedure is further divulged in Appendix A. Intermediate evaluations are numerically summarized in Table 6.

Table 6. Filtered Subcase 3 of Constant Speed Envelope Deviation (g's): Reduced Number of Accelerometers as Input

Filtered Case	10Z RMSD	13Z RMSD	16Z RMSD	10Z STDEV	13Z STDEV	16Z STDEV
Filtered Case 1 (17Z 21Z 9Z deleted)	0.5206	0.7231	0.3325	0.0515	0.0250	0.0358
Filtered Case 2 (17Z 9Z deleted)	0.4396	0.5111	0.3072	0.0383	0.0230	0.0287
Filtered Case 3 (17Z 21Z deleted)	0.4940	0.4996	0.3287	0.0513	0.0083	0.0334
Filtered Case 4 (21Z 9Z deleted)	0.4867	0.4473	0.2992	0.0558	0.0079	0.0268
Filtered Case 5 (9Z deleted)	0.4946	0.4196	0.1755	0.0095	0.0037	0.0086
Filtered Case 6 (9Z 4Z deleted)	0.4929	0.4232	0.1878	0.0098	0.0037	0.0100
Filtered Case 7 (8Z 9Z deleted)	0.5004	0.4032	0.1768	0.0095	0.0036	0.0089

The effect of the accelerometer deletions was also gauged by the percent difference calculated in association to each of the seven case studies versus the validation data. Equation 7 was used to calculate the deviation. A summary of the data deviation is shown in Table 7 below.

R refers to the result data in Table 6, and O refers to original data in Table 5 Subcase 3 of Constant Speed Envelope.

$$\%Difference = \frac{(R-O)}{(R+O)/2} * 100\% \qquad (7)$$

Table 7. Filtered Data Percent Difference

Filtered Case	10Z RMSD	13Z RMSD	16Z RMSD	10Z STDEV	13Z STDEV	16Z STDEV
Filtered Case 1 (17Z 21Z 9Z deleted)	6.8%	48.1%	63.4%	138.2%	149.1%	126.1%
Filtered Case 2 (17Z 9Z deleted)	-10.1%	14.3%	56.2%	121.1%	145.3%	111.7%
Filtered Case 3 (17Z 21Z deleted)	1.6%	12.1%	62.3%	138.0%	78.1%	121.7%
Filtered Case 4 (21Z 9Z deleted)	0.1%	1.0%	53.7%	142.2%	74.1%	107.0%
Filtered Case 5 (9Z deleted)	1.7%	-5.4%	1.8%	1.0%	1.1%	5.7%
Filtered Case 6 (9Z 4Z deleted)	1.3%	-4.5%	8.5%	4.4%	1.7%	21.2%
Filtered Case 7 (8Z 9Z deleted)	2.8%	-9.4%	2.5%	1.4%	-0.8%	9.2%

The iterative method implemented during the study provided insight on how the location of accelerometers effects the overall correlation between sea trial and model data. The greatest deviation occurred with the changes to the presence of the port and starboard accelerometers. Graphical representation of the final evaluation is provided in Figure 12 below.

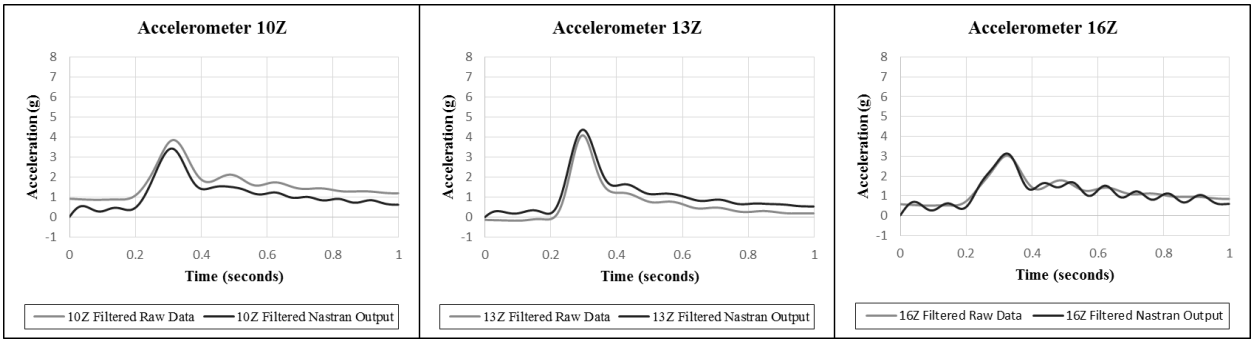

Figure 12. Filtered Comparisons after Accelerometers 8Z and 9Z Deleted

Alteration of quantity and placement for enforced acceleration input using sea trial data resulted in a 1.95% reduction in root mean square deviation when compared to the best-correlating case of the finite element model validation investigation, based upon percent difference. The study was able to prove that the quantity of accelerometers can be reduced and still yield accurate results.

In summary, the removal of 8Z and 9Z displayed the best correlation when compared to the other 6 cases investigated. The removal of 8Z and 9Z also displayed a better correlation in terms of root mean square deviation when compared to the filtered raw data. However, none of the seven cases investigate yield better correlation in terms of standard deviation when compared to the filtered raw data.

4.2 Displacement

Deformation and fringe plots of the planing craft near the time of peak acceleration outputs from 10Z, 13Z, and 16Z are shown in Figures 13 and 14. The vessel was traveling at 20.3 knots in waves heights of 3.4 feet. Max displacement of 0.811 inches was found at Node 372. Additional deformation plots from varying time stamps are provided in Appendix C. Many of the same steps required for obtaining acceleration output were taken to retrieve displacement output, with a few key differences. During Step 6 of Appendix A, **Displacements** was selected instead of **Accelerations**, for Result Type, and request for output of the full finite element model was made by selecting **All FEM**, instead of **1**, for Group(s)/SET.

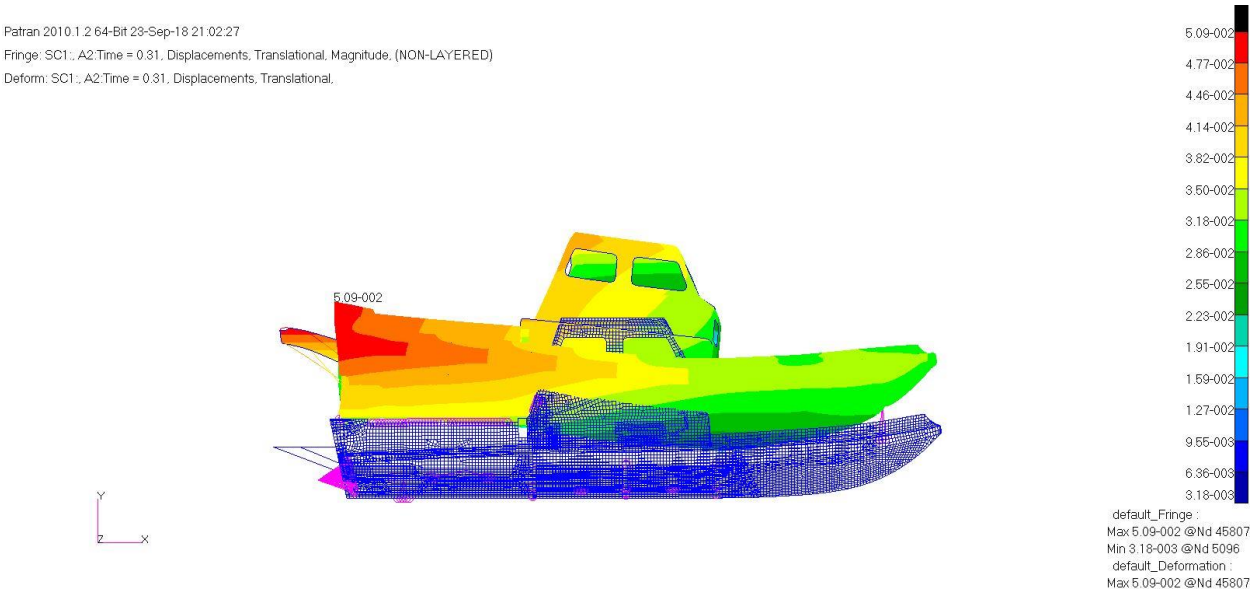

Figure 13. Side View of Deformation plot at 0.31 seconds

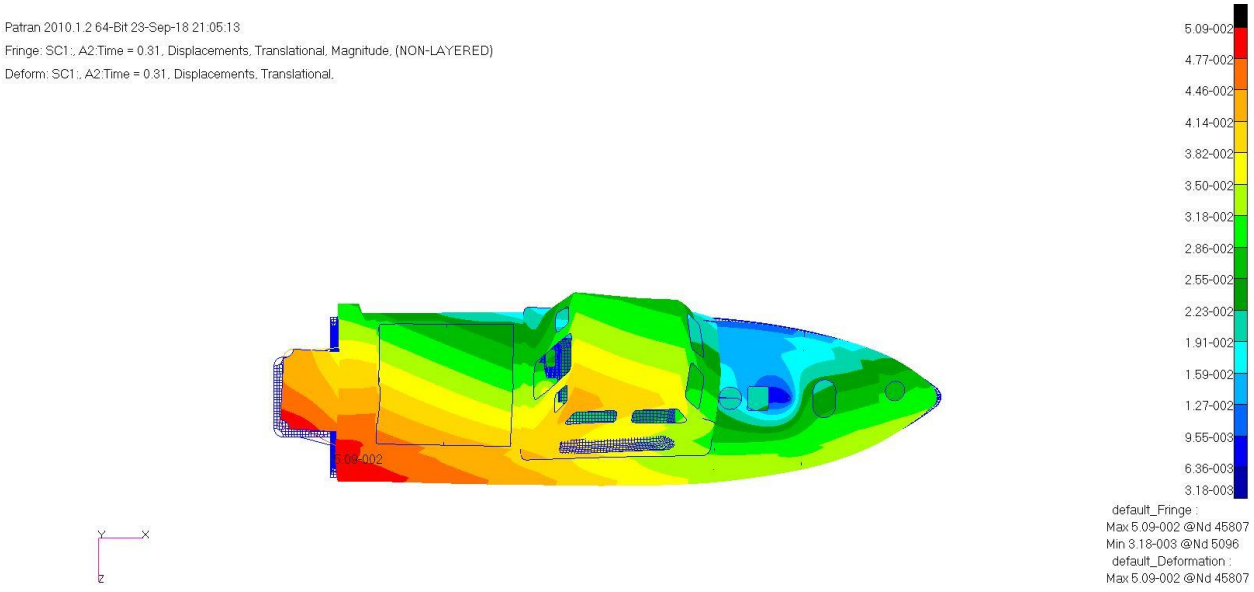

Figure 14. Top View of Deformation plot at 0.31 seconds

4.3 Cabin Sub-model Analysis

Isolation of the pilot cabin was achieved through successive element reduction. In order to realize the isolated condition, the pilot cabin was separated from the main deck of the RIB. This stage of the investigation required the deletion of elements surrounding an approximate 75.5 inch by 115-inch area within PATRAN. The result of said action is shown in Figure 15. Isolation of the pilot cabin in this manner yielded a RIB model with the locations of nodes associated with accelerometers 10Z, 13Z, and 16Z still intact for output purposes. It should be noted that although 10Z, 13Z, and 16Z remained intact, their output nodal number was altered from that of the previous investigations following the equivalence procedure to the remaining finite element model.

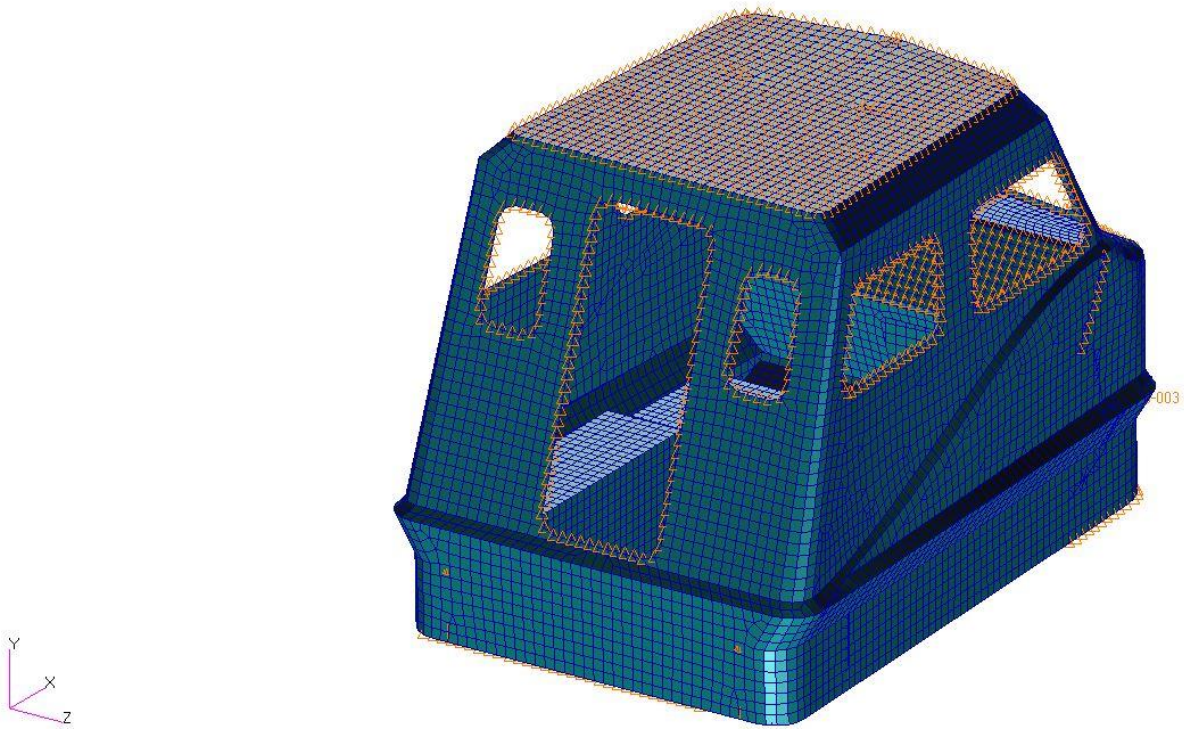

Figure 15. Isolated Pilot Cabin

Due to the overall correlation found when conducting analysis of the Constant Speed Envelope at 20.3 knots and significant wave height of 3.4 feet, and for consistency, its data was used as a model dataset during completion of the isolated pilot cabin analysis. Accelerometer data was extracted from the full boat model in order to represent functioning accelerometers during sea trial data collection. The spectrum plot for the Constant Speed Envelope at 20.3 knots and significant wave height of 3.4 feet is displayed in Figure 16. The plot shows that the majority of major amplitude conditions occur until a frequency of 10 Hertz and 13 Hertz. In order to capture the accelerations associated with the rigid body of motion of the Constant Speed envelope subcase 3, the data was filtered separately at 10 Hertz and 13 Hertz.

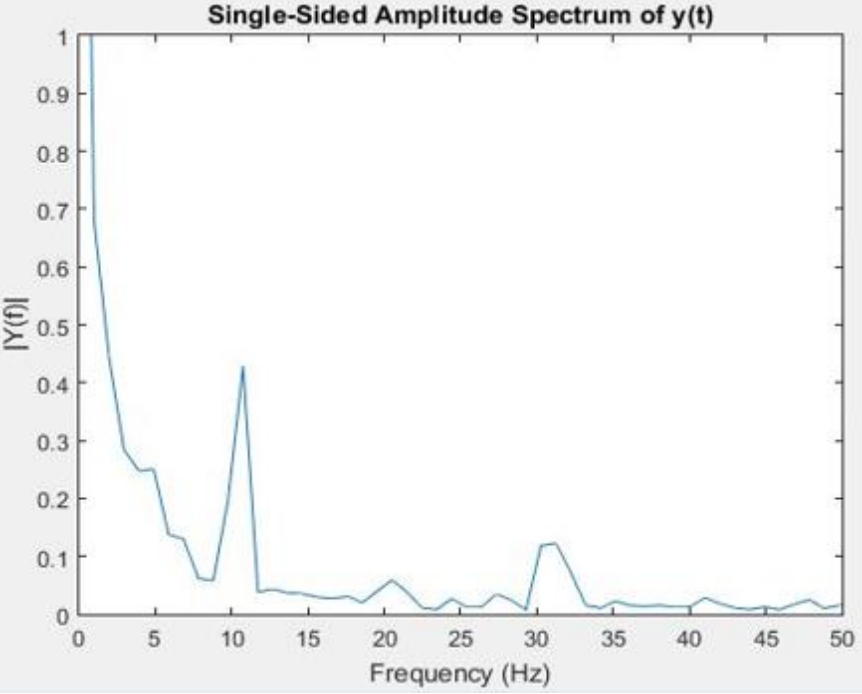

Figure 16. Subcase 3 of Constant Speed Envelope: 16Z Pilot Cabin Spectrum Plot

In order to enforce acceleration upon an isolated pilot cabin, selection of appropriate locations for base excitation accelerometers was required for implementation. Ideal locations for the nodes were assumed to be at the top of bulkheads, beneath the cabin, for the bulkheads' rigidity. Due to the way in which the bulkhead intersections are offset from the base of the pilot cabin, as shown in Fig. 17, the locations of the nodes on the bulkheads were not within the pilot cabin section to be analyzed. Therefore, the nodes on the bulkheads were approximated with nodes on the cabin, which have similar x-y-z coordinates. Seven nodes at the intersection of the transverse and longitudinal bulkheads were approximated with nodes along the underside of the pilot cabin. Results from the full boat sensitivity study aided in the selection of the seven approximation nodes. Figure 18 is an underside view of the pilot cabin and shows the location of the seven nodes selected, marked by a red dot. The nodes are directly beneath the pilot cabin deck and directly above the transverse bulkheads. Due to the sensitivity study showing better correlation with a symmetric port and starboard acceleration input, the port and starboard each have three nodes. Due to the sensitivity study showing minimum correlation effect following the deletion of longitudinal nodes and the desire to use a minimum amount of data, only one longitudinal node was selected for input. The acceleration at the intersection of the transverse and longitudinal bulkheads served as a benchmark for the pilot cabin nodes to meet and a justification of the approximation made to continue this study. The assumption regarding similar acceleration values in a region near the intersection of the longitudinal and transverse beams was verified graphically and numerically, the latter through the calculations of root mean square deviation and standard deviation for the seven nodes selected. The deviation following approximation is minimal, as discussed below.

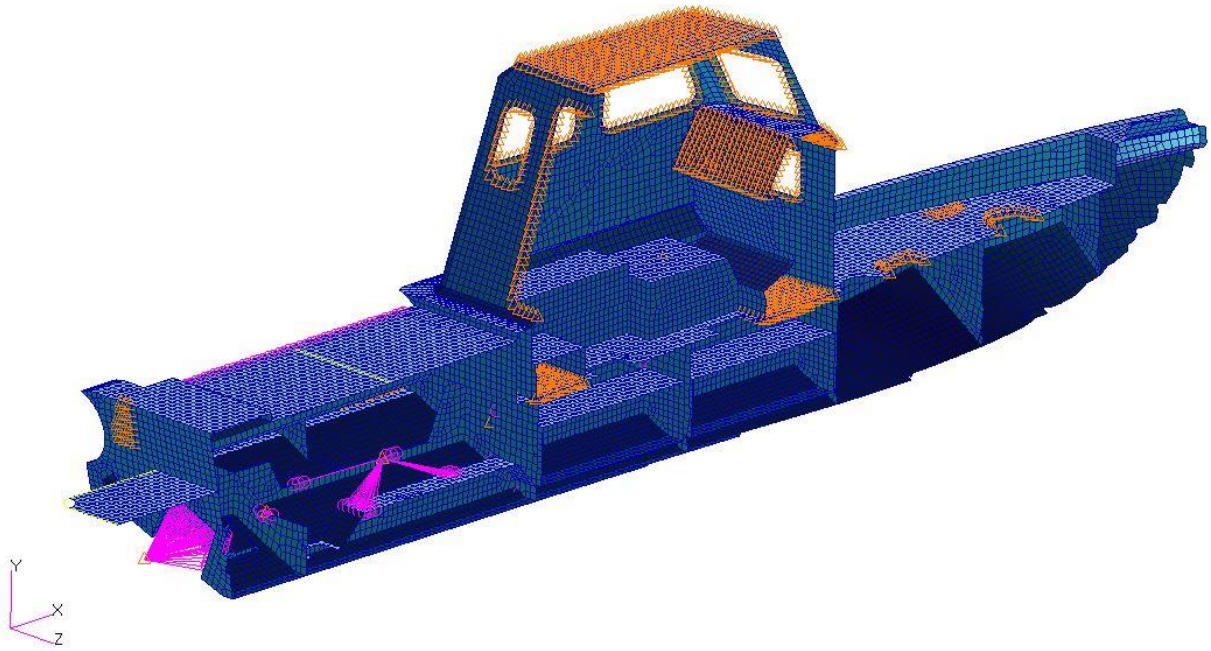

Figure 17. Side-View of 11-meter Cabin RIB Model Transverse Bulkheads

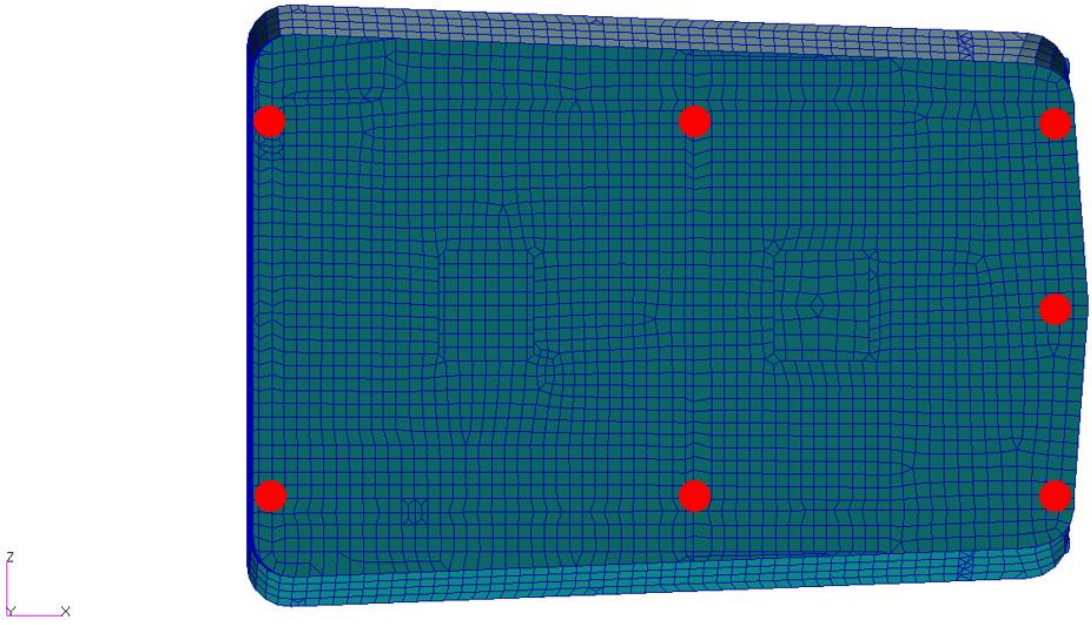

Figure 18. Seven Node Locations on 11-meter Cabin RIB Model

Original Intersections were used for comparison purposes to verify the assumption. The difference in output between the bulkhead intersections and their approximations was found to be negligible, with a maximum root mean square deviation and standard deviation of 0.065 g and 0.0015 g respectively. Graphical representations of their correlation are depicted in Appendix D, for both the 10-Hertz and 13-Hertz investigations. The acceleration profiles of the nodal intersection approximations are approximately the same as the acceleration profiles of the original intersection nodes.

The final evaluation utilized the approximated nodal outputs for enforced acceleration. In order to simulate the dynamic effects, the time-dependent accelerations were input through PATRAN and solved by MSC NASTRAN, a method which is further divulged in Appendix A. Dynamic responses at selected accelerometers, 10Z, 13Z, and 16Z, were compared against both acceleration data collected during sea trials and acceleration data collected during the full-boat model validation investigation, as shown in Figures 19 and 20.

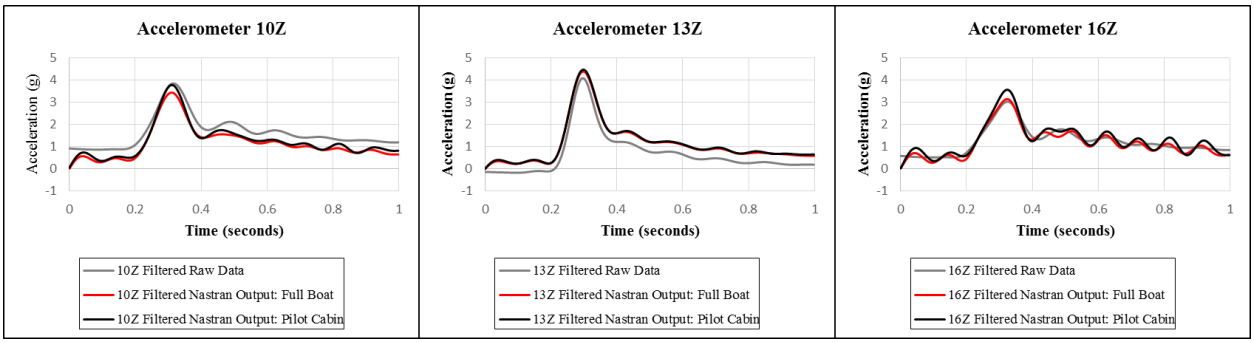

Figure 19. Pilot Cabin Output Comparison with Data Filtered at 10 Hertz

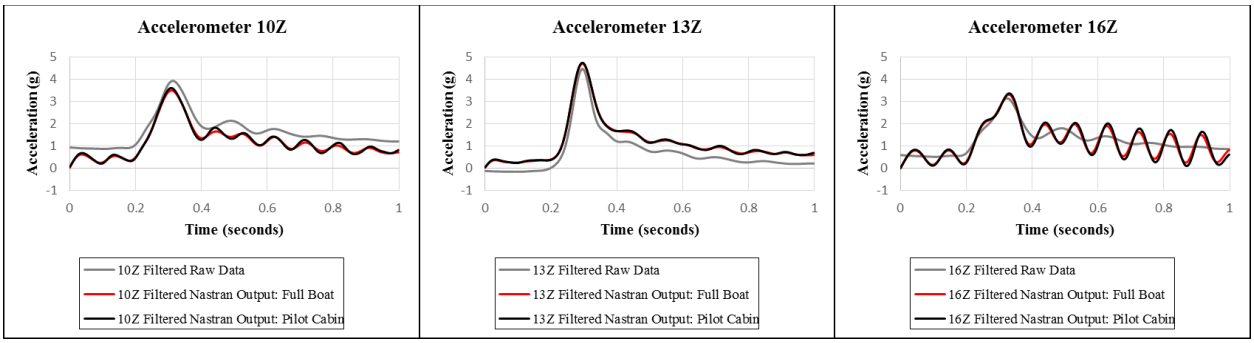

Figure 20. Pilot Cabin Output Comparison with Data Filtered at 13 Hertz

When filtered at a greater frequency, more motion was induced during enforced acceleration. Results show that there was a 16.5% reduction in standard deviation when filtered at 13 Hertz. Demonstration of the isolated pilot cabin provides proof that accuracy in output data can be maintained through a reduced test model.

In addition to maintaining output correlation with sea trial data, by localizing the scope of the investigation stress contour plots of the pilot cabin, such as Figures 21 and 22, were realized. Local stress magnitude on the pilot cabin was obtained and can be used to aid in design changes. The maximum stress of the elements for both faces of the element are shown. The designation Z2 corresponds to the top face associated with the element normal vector, and the designation Z1

corresponds to the bottom face opposite the face normal. Figure 21 shows that there is a maximum Von Mises stress of 6.28 psi. Figure 22 shows that there is a maximum Von Mises stress of 6.48 psi.

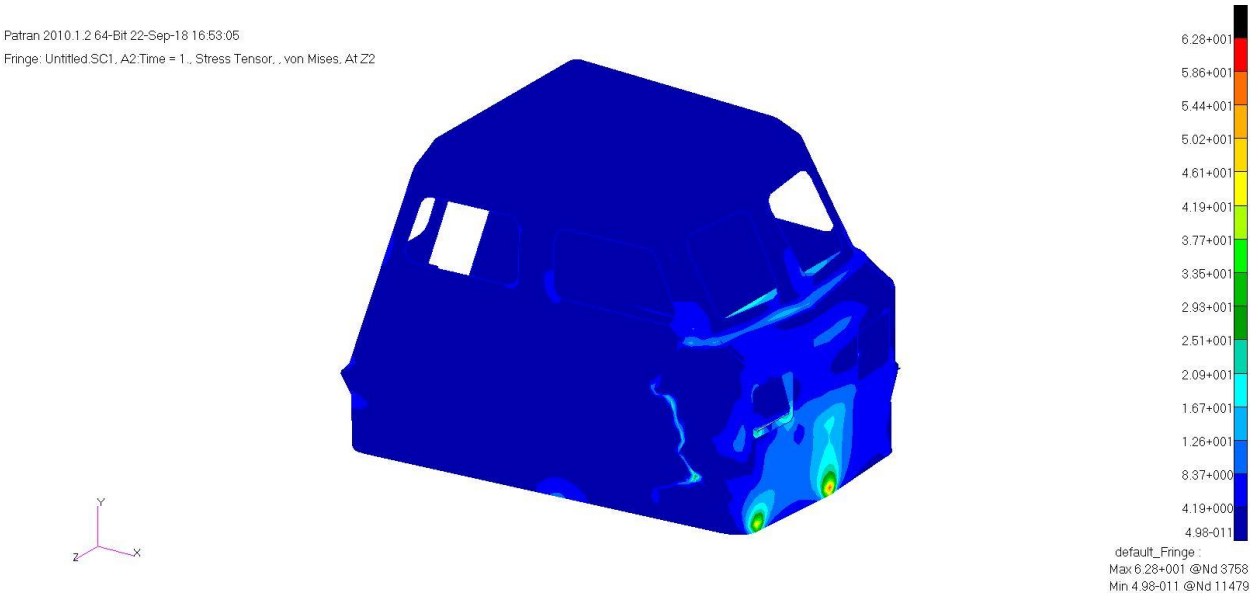

Figure 21. Stress Contour Plot using Data Filtered at 13 Hertz: Z2 Maximum Stress

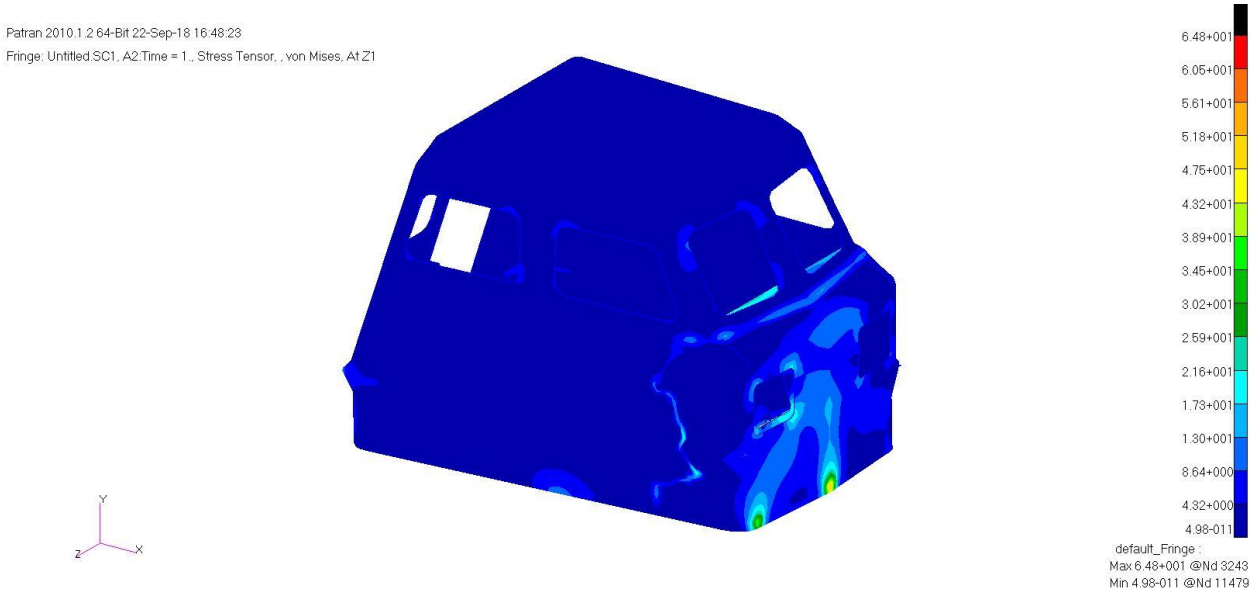

Figure 22. Stress Contour Plot using Data Filtered at 13 Hertz: Z1 Maximum Stress

The final analysis of the cabin sub-model included two parts. Acceleration and stress at the finite element model seat pedestals were investigated. Node 5838 is located at the port seat pedestal and Node 4957 is located at the starboard seat pedestal. The acceleration plots for both locations are shown in Figure 23. Unlike the previous locations investigated, the lumped mass developed to represent the seats began to oscillate due to the wave impact.

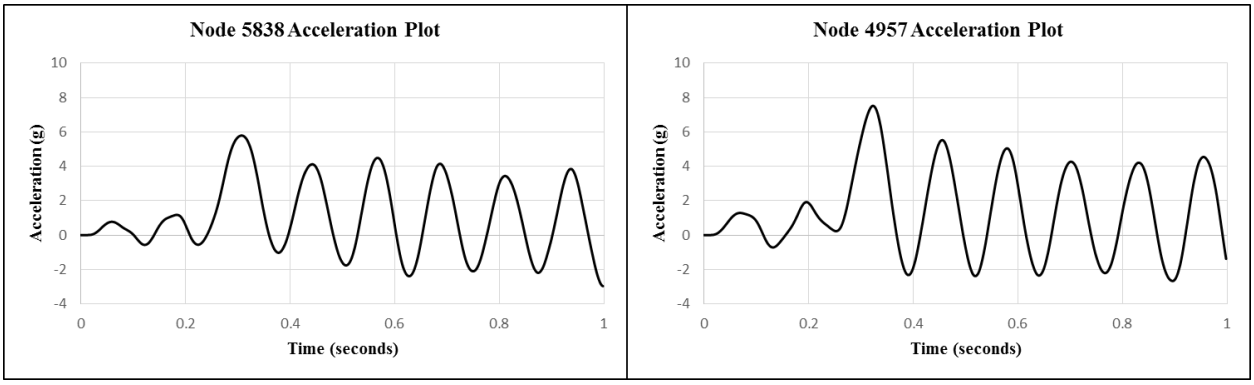

Figure 23. Node 5838 and Node 4957 Acceleration Plots

With stress being the cause of injury, the second step was to investigate the resulting stress profile that would be felt at the seat pedestals. In order to realize the stress profiles at the seat pedestals, shown in Figure 24, the stress profiles of the four CQUAD elements surrounding each of the two nodes were averaged. Figures 25 and 26 show the maximum stresses developed at the top and bottom of the shell elements surrounding Node 5838 respectively. Figures 27 and 28 show the maximum stresses developed at the top and bottom of the shell elements surrounding Node 4957 respectively.

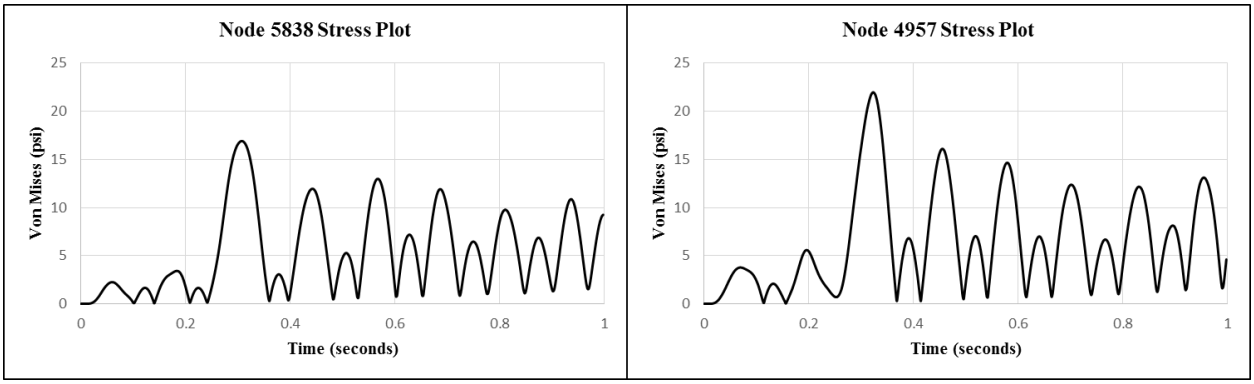

Figure 24. Node 5838 and Node 4957 Stress Plots

Due to the fact that Von Mises stress is positive, stress peaks are followed by smaller spikes. This occurs throughout the stress profile plot. The stress output for the Starboard Seat Pedestal was the same for both faces of the element. However, the stress output for the Port Seat Pedestal showed a minor difference of 0.2 psi.

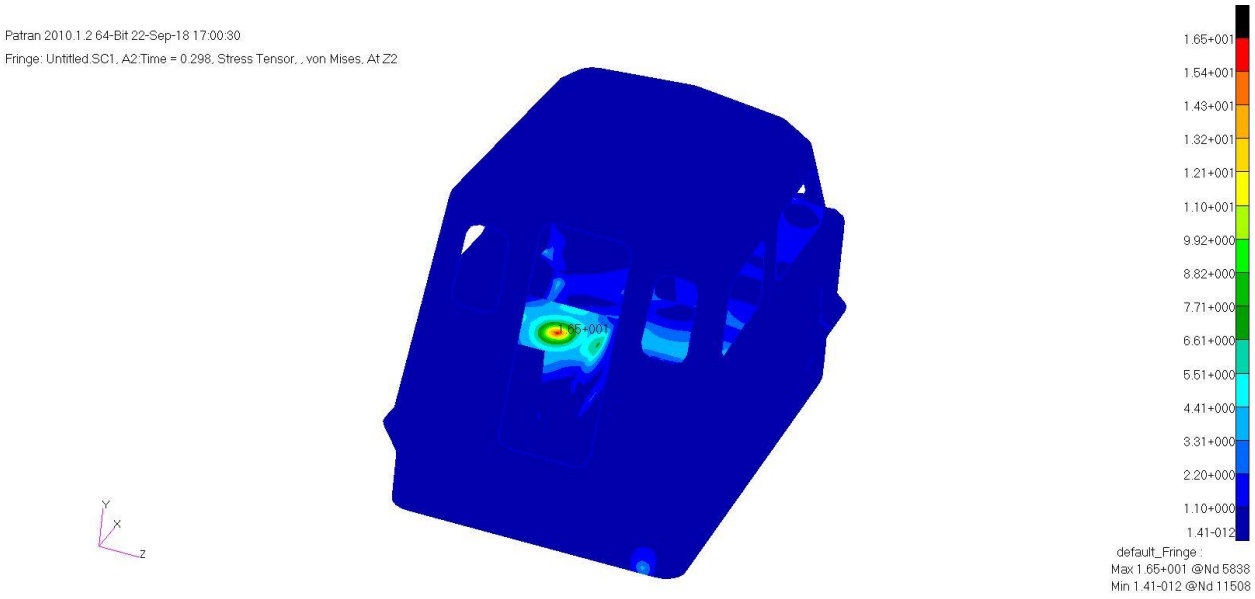

Figure 25. Cabin Stress Contour Plot at Z2: Port Seat Pedestal Node 5838

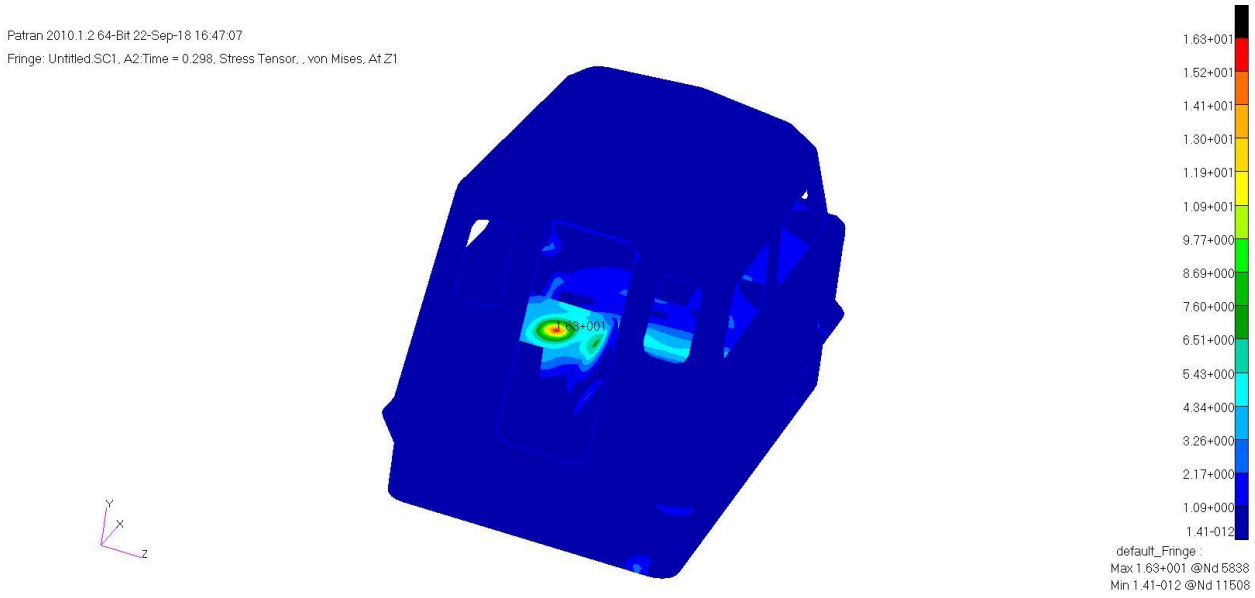

Figure 26. Cabin Stress Contour Plot at Z1: Port Seat Pedestal Node 5838

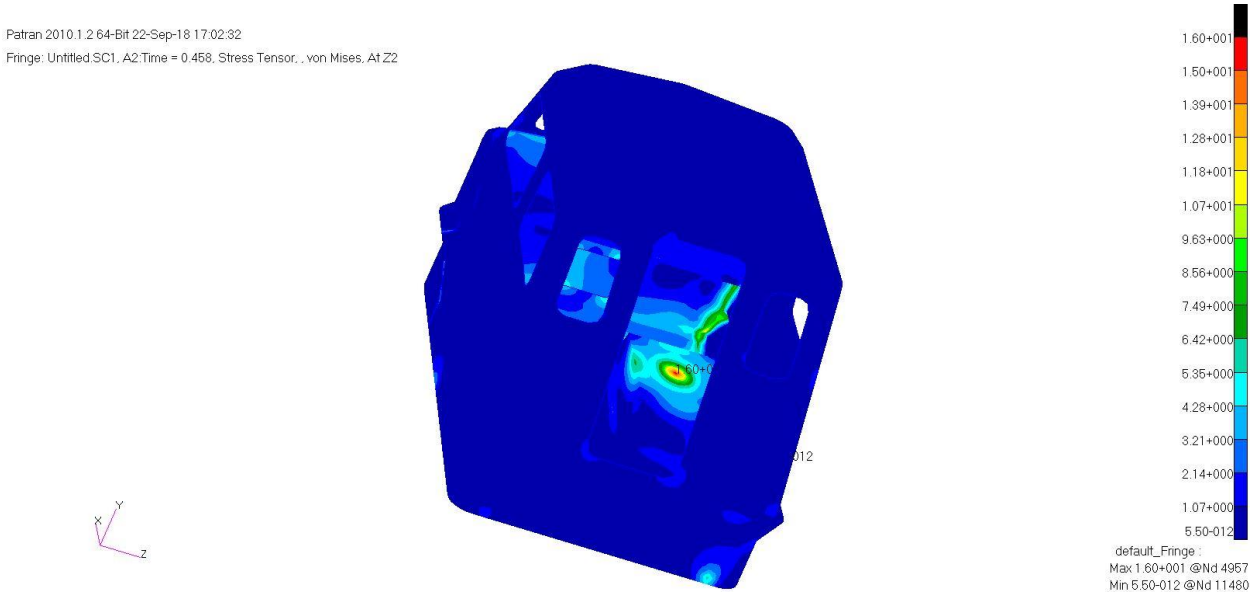

Figure 27. Cabin Stress Contour Plot at Z2: Starboard Seat Pedestal Node 4957

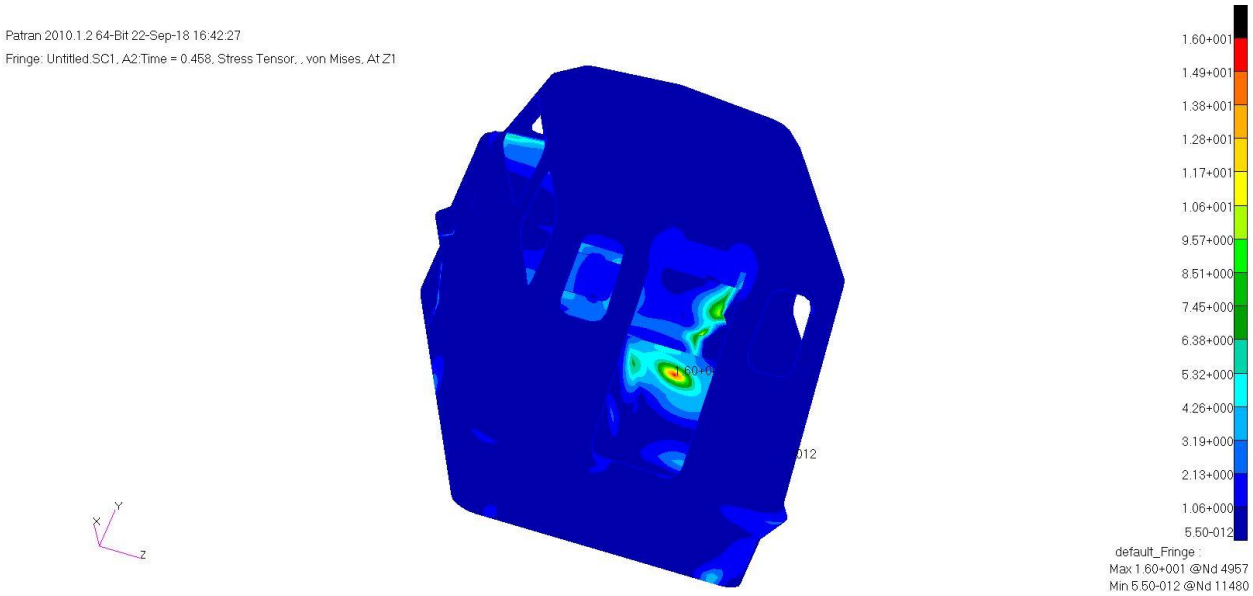

Figure 28. Cabin Stress Contour Plot at Z1: Starboard Seat Pedestal Node 4957

CHAPTER 5

5. CONCLUSION AND RECOMMENDATIONS

The development of methods and procedures to better understand the dynamic response of high speed planing hulls to wave impacts are necessary in order to mitigate risk to crew and equipment. In the current work, the approach was the use of acceleration data as an input. Investigations into the dynamic response of a high speed planing craft were completed by enforcing acceleration data at specific nodes and recording the resulting acceleration output at the bottom, midsection, and top of the pilot cabin. The resulting acceleration data was then validated through comparison to the acceleration output from sea trials. More specifically, this thesis demonstrated that the use of the finite element model is acceptable for dynamic simulation of the 11MRB0503 by showing that the rigid body accelerations output from the model correlate with the rigid body accelerations recorded during full scale sea trials. This was made possible through the use of the StandardG algorithm.

The integration of captured accelerometer data and developed finite element data provided the ability to estimate cabin stresses without the use of strain gauges or pressure sensors. Separately, the two methods provide researchers with valuable information. However, when combined together the methods have the ability to provide further insight not witnessed through the use of either method alone. The integration of the two types of data yielded additional information not obtainable from either data type alone.

An acceptable procedure for modeling dynamic responses of a high speed planing craft was developed. The method provides insight into where modifications are necessary and how modifications will perform under varying sea states. The methods and procedures used

throughout this work can be utilized on other structures, attached to large rigid structures (i.e. hull, bulkheads, deck plates etc.), were conducting live tests is costly.

An actual comparison of the structural changes due to wave impact could not be completed since strain gauges or pressure sensors were not mounted before sea trials were conducted. It is recommended that such steps be taken to allow for a second means of validation. Results are largely dependent upon the accuracy of the initial finite element model. Greater efforts placed in the accuracy of the pilot cabin would yield more accurate results when compared to the sea trial data. Future investigations should focus on local modifications and their resulting effects. Although large stress concentrations or deflections were not realized, the approach is documented and can be carried out by future researchers whom lack strain gauge or pressure transducer data from their experimental craft or structure.

REFERENCES

Allen, R. G., Jones, R. R., & Taylor, D. W. (1978). A Simplified Method for Determining Structural Design-Limit Pressures on High Performance Marine Vehicles. In *Proceedings of the AIAA/SNAME Advanced Marine Vehicle Conference*. San Diego, CA.

Bampton, M. C., & Craig, J. R. (1968). Coupling of Substructures for Dynamic Analyses. *AIAA Journal, 6*(7), 1313-1319. doi:10.2514/3.4741

Carrica, P. M., Huang, J., Noack, R., Kaushik, D., Smith, B., & Stern, F. (2010). Large-scale DES Computations of the Forward Speed Diffraction and Pitch and Heave Problems for a Surface Combatant. *Computers and Fluids, 39,* 1095-1111.

Chandrupatla, T. R., & Belegundu, A. D. (2012). *Introduction to Finite Elements in Engineering*. Upper saddle river: Prentice hall.

Cho, D. S., Kim, B. H., Kim, J., Vladimir, N., & Choi, T. M. (2016). Frequency response of rectangular plates with free-edge openings and carlings subjected to point excitation force and enforced displacement at boundaries. *International Journal of Naval Architecture and Ocean Engineering, 8*(2), 117-126. doi:10.1016/j.ijnaoe.2015.06.001

Clough, R. W., & Penzien, J. (1975). *Dynamics of Structures*. New York, NY: McGraw-Hill.

Corbishdale, A. J. (2014). *Finite Element Model Creation and Modal Analysis of a Zodiac H1110 AFT IO CABIN RIB for the Wave-Slam Phenomenology and Transmissibility of a High-Speed Planing Craft Core R&D Project* [Scholarly project]. Retrieved 2015.

Davis, M. D. (2011). *Transient Finite Element Analysis of a Base Excited Frame on a Six DOF Motion Simulator to Simulate Wave Slamming* (Master's thesis). Old Dominion University.

Davis, M., Tedesco, S., Huynh, T., & Hou, G. (2012). Finite Element Transient Analysis of Flexible Structure under Wave Slamming Environment. In *Proceedings of the 4th International Forum on Systems and Mechatronics* (pp. 214-231). Virginia Beach, VA.

Faltinsen, O. M. (2005). *Hydrodynamics of High-Speed Marine Vehicles*. New York, NY: Cambridge University Press.

Flanigan, C. C. (1994). Accurate Enforced Motion Analysis using MSC/NASTRAN Super-elements. In *1994 MSC/NASTRAN World Users Conference*. Orlando, FL.

Fridsma, G. (1971). *A Systematic Study of the Rough Water Performance of Planing Boats – Irregular Waves – Part II* (Rep.). Hoboken, NJ: Stevens Institute of Technology.

Garme, K., & Rosen, A. (2003). Time-Domain Simulations and Full-Scale Trials on Planing Craft in Waves. *International Shipbuilding Progress, 50*(3), 177-208.

Grimsley, J., Liu, Y., & Hou, G. (2010). An Examination of the Statistical Behavior of Planing Craft Peak Vertical Accelerations in Irregular Waves. In *Proceedings of the 29th American Towing Tank Conference* (pp. 31-39). Annapolis, MD.

Hoggard, M., & Jones, M. (1980). Examining Pitch, Heave, and Accelerations of Planing Craft Operating in a Seaway. In *High-Speed Surface Craft Exhibition and Conference*. Metropole, Brighton, U.K.

Joo, H. K., Mohamad, M. A., & Sapsis, T. P. (2017). Extreme Events and Their Optimal Mitigation in Nonlinear Structural System Excited by Stochastic Loads: Application to Ocean Engineering Systems. *Ocean Engineering, 142*, 145-160.

Liu, Y., & Lu, Z. (2010). Methods of enforcing earthquake base motions in seismic analysis of structures. *Engineering Structures, 32*(8), 2019-2033. doi:10.1016/j.engstruct.2010.02.035

Ma, S., & Mahfuz, H. (2012). Finite Element Simulation of Composite Ship Structures with Fluid Structure Interaction. *Ocean Engineering, 52,* 52-59.

Murphy, H. P., & Planchak, C. J. (2015). *Description of the Rough-Water Dataset Captured on a Shallow-Vee Hull* (pp. 1-85, Rep.). West Bethesda, MD: Naval Surface Warfare Center, Carderock Division.

Razola, M., Olausson, K., Garme, K., & Rosen, A. (2016). On High-Speed Craft Acceleration Statistics. *Ocean Engineering, 114,* 115-133.

Razola, M., Rosen, A., & Garme, K. (2014). Allen and Jones Revisited. *Ocean Engineering, 89,* 119-133.

Reddy, J. N. (1984). *An Introduction to the Finite Element Method* (Second ed.). McGraw Hill.

Riley, M. R., & Coats, T. W. (2013). *The Simulation of Wave Slam Impulses to Evaluate Shock Mitigation Seats for High-Speed Planing Craft* (pp. 1-90, Tech.). West Bethesda, MD: Naval Surface Warfare Center, Carderock Division.

Riley, M. R., & Peterson, S. M. (2017). *The Use of Shock Isolation Mounts in Small High-Speed Craft to Protect Equipment from Wave Slam Effects* (pp. 1-70, Tech.). Bethesda, MD: Naval Surface Warfare Center, Carderock Division.

Riley, M. R., Coats, T. W., Haupt, K. D., & Jacobson, D. R. (2010). The Characterization of Individual Wave Slam Acceleration Responses for High Speed Craft. In *Proceedings of the 29th American Towing Tank Conference* (pp. 31-39). Annapolis, MD.

Riley, M. R., Murphy, H. P., & Coats, T. W. (2016). An Integrated Approach for Developing Rough Water Methodologies for Small High-Speed Craft Structure, Equipment, Shock Isolation Seats and Human Performance At-Sea. In *The 10th Symposium on High Performance Marine Vehicles*. Cortona, Italy.

Rosen, A., & Garme, K. (2004). Model Experiment Addressing the Impact Pressure Distribution on Planing Craft In Waves. *International Journal of Small Craft Technology*.

Rosen, A. (2005). Impact Pressure Distribution Reconstruction from Discrete Point Measurements. *International Shipbuilding Progress, 52*(1), 91-107.

Scovazzi, G., Song, T., & Zheng, X. (2017). A Velocity/Stress Mixed Stabilized Nodal Finite Element for Elastodynamics: Analysis and Computations with Strongly and Weakly Enforced Boundary Conditions. *Computer Methods in Applied Mechanics and Engineering, 325*(1), 532-576.

Sukas, O. F., Kinaci, O. K., Cakici, F., & Gokce, M. (2017). Hydrodynamic Assessment of Planing Hulls using Overset Grids. *Applied Ocean Research, 65*, 35-46.

Trenor, S., Sanders, M., Johnson, B. K., Michaeli, J. G., & Hou, G. (2015). *Investigation into Dynamic Response Modeling for 11m RHIB with Forced Acceleration* (p. 1, Poster). Arlington, Virginia.

VanDerwerken, D., & Judge, C. (2017). Statistical Analysis of Vertical Accelerations of Planing Craft: Common Pitfalls and How to Avoid Them. *Ocean Engineering, 1*(39), 265-274.

Volpi, S., Diez, M., Sada-Hosseini, H., Stern, F., Thodal, R. S., Grenestedt, J. L., & Kim, D. -. (2017). Composite Bottom Panel Slamming of a Fast Planing Hull via Tightly Coupled Fluid-Structure Interaction Simulations and Sea Trials. *Ocean Engineering, 143*, 240-258.

Xie, H., Ren, H., Qu, S., & Tang, H. (2018). Numerical and Experimental Study on Hydroelasticity in Water-entry Problem of a Composite Ship-Hull Structure. *Composite Structures, 201*, 942-957.

Yang, C., & Huang, F. (2016). An Overview of Simulation-based Hydrodynamic Design of Ship Hull Forms. *Journal of Hydrodynamics, 6*, 947-960.

Yang, L. (2018). One-Fluid Formulation for Fluid-Structure Interaction with Free Surface. *Computational Methods in Applied Mechanics and Engineering, 332*, 102-135.

Appendix A – PATRAN and NASTRAN Enforced Acceleration Procedure

STEP 1: Double-Click on **PATRAN** 

.

Click on **OK** to accept the Message.

Option 1: Click on **File>Open>** then Double-Click on**> Appendix A> Cabin_No_Boundary** for isolated cabin analysis.

Option 2: Click on **File>Open>** then Double-Click on**> Appendix A> Acceleration** for full boat analysis.

STEP 2: Click on **Loads/BCs>Create Non-Spatial** 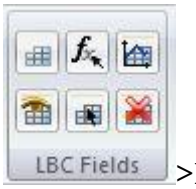

>Input Data…>Import/Export….

At this point, each of the seven approximated nodal location's data are imported, if conducting isolated cabin analysis. If conducting full boat analysis, each of the eleven nodal location's data are imported. All of the data are in the form of CSV files. An example is provided below using file name "11073856".

Click on **11073856** 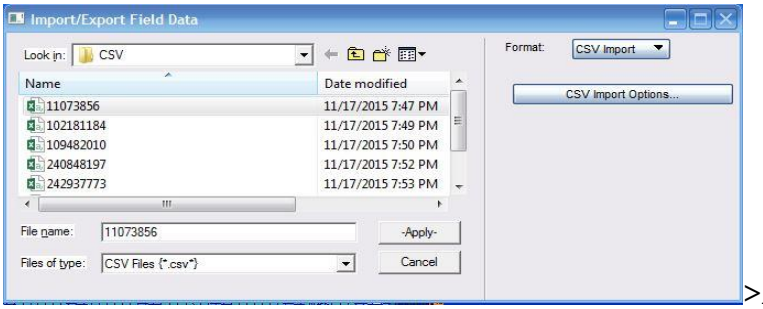

>Apply>OK.

Create a Field Name 

> Click **Apply**.

If correctly imported, ‘Existing Fields’ should show the ‘Field Name’ previously created as shown here 

. The procedure is repeated for the remaining CSV files.

Remember to update the ‘Field Name’ before importing a new CSV file.

STEP 3: Click on **Create Load Case** 

>Untitled.SC1>OK>Time Dependent.

Set ‘Load Case Scale Factor’ to **1.0**.

The interface should resemble 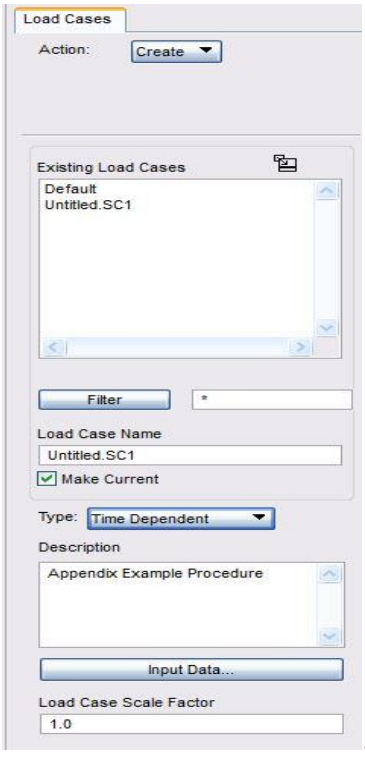

. Click **Apply>Yes** Overwrite.

STEP 4: Click on **Acceleration** 

>Input Data….

Type **<,1.,>** under ‘Trans Accel<A1 A2 A3>’ and Click on **11073856** for application to ‘Time/Freq. Dependence’.

The interface should resemble 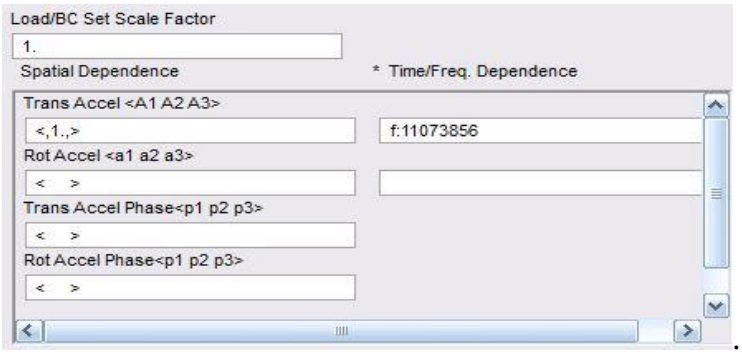

. Click on **OK>Select Application Region…>FEM**.

Type the desired nodal location for the enforced acceleration data to be applied

. Click on **Add>OK.**

Create a New Set Name 

>Click **Apply**. This acceleration procedure is repeated for each CSV file initially imported. If correctly enforced, ‘Existing Sets’ should show

. Remember to update the ‘New Set Name’ and ‘Select Application Region…’ before applying a new set of input data. All data is enforced in the manner described above.

In order to remove the enforced data set, as utilized during the Sensitivity Study, the user selects **Delete** for ‘Action:’ and **Acceleration** for ‘Object:’

Click on the data that should be deleted under ‘Existing Sets’. The selected set of data should appear under ‘Sets to be Deleted’ and should resemble 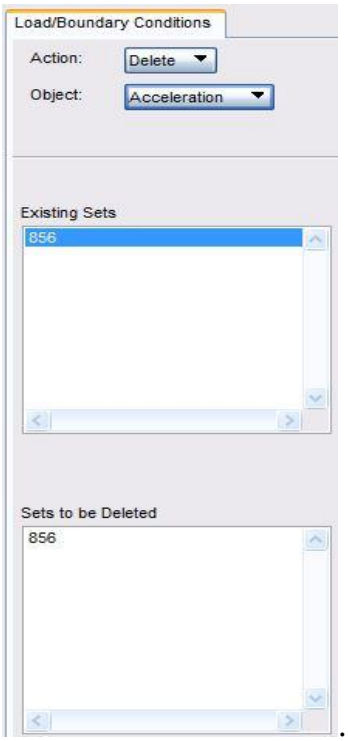

. Click **Apply**. This step is repeated for any data set deemed unnecessary for the particular analysis.

In order to analyze the FE model, a group is created for the critical outputs. As an example, accelerometers 10z, 13z, and 16z are considered to be the critical outputs.

STEP 5: Click on **Group>Create…>** type a New Group Name 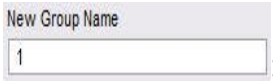

>type the nodal locations that represent accelerometers 10z, 13z, and 16z.

Under ‘Entity Selection’ 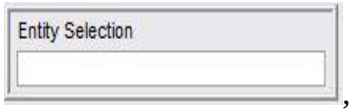

, type **node 9088 200 10043** when using the Cabin FE model and type **node 25872 8508 18747** when using the Full Boat FE model. Click

Apply. If correctly implemented, the New Group Name will appear under 'Existing Group Names' as shown here 

.

STEP 6: Click **Analysis**. The Analysis tab should show 

.

Click on **Solution Type…>TRANSIENT RESOPNSE>** 

>OK.

Click on **Subcases…>Untitled.SC1>Subcase Parameters…>DEFINE TIME STEPS…>**

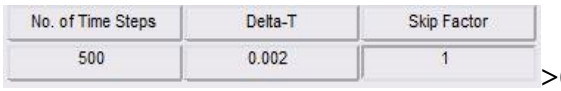

>OK>OK>Apply>Cancel.

Click on **Subcases…> Untitled.SC1>Output Requests…>** 

>Accelerations for 'Select Result Type'**>1** for 'Select Group(s)/SET'.

The 'Output Requests' section should display 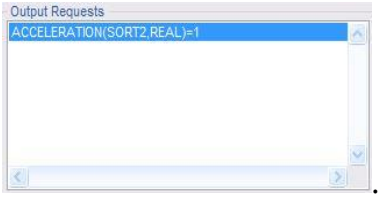

.

Click on **OK>Apply>Yes>Cancel**.

Click on **Subcase Select…>Unselect All>Untitled.SC1>OK**.

In order to avoid confusion in the future, create a new 'Job Name' as shown here

. Click on **Apply>OK>OK**. If implemented correctly,

‘Available Jobs’ should display 

and a new BDF file should have been generated in the same folder that was opened to initiate the procedure.

Computations in NASTRAN can commence after a successful BDF file is generated with the desired enforced data.

STEP 7: Double-Click on **NASTRAN** 

.

Click on **Appendix A_Procedure>Open>Run**. This action will cause the generation of an f06 file with the acceleration outputs previously specified.

Appendix B – MATLAB Data Plots

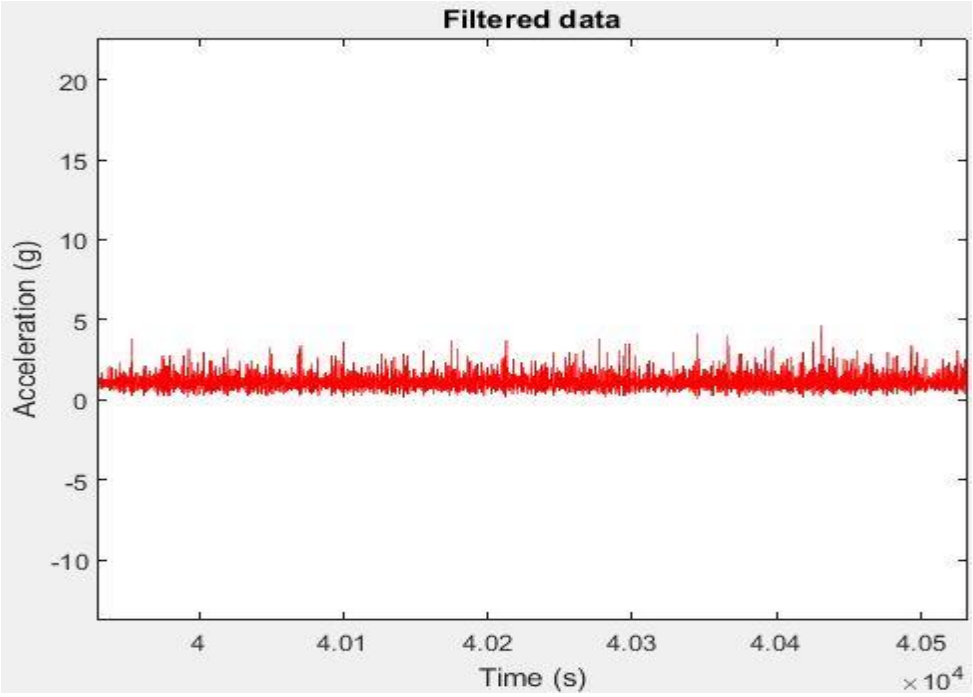

Figure B1. Accelerometer 1Z Filtered Data Plot

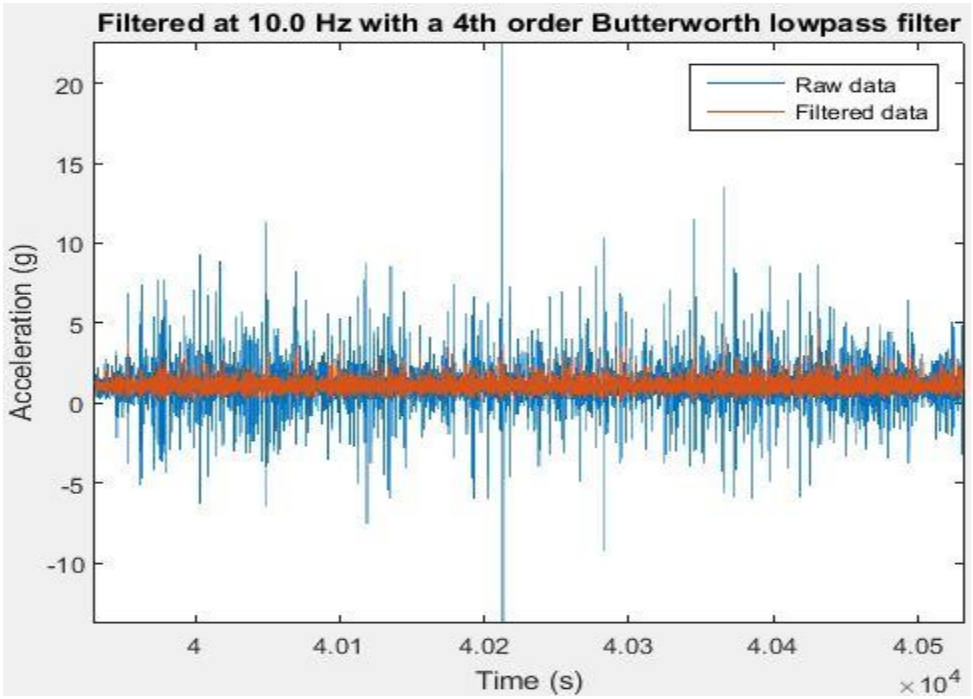

Figure B2. Accelerometer 1Z Data Comparison Plot

Appendix C – Deformation Plots

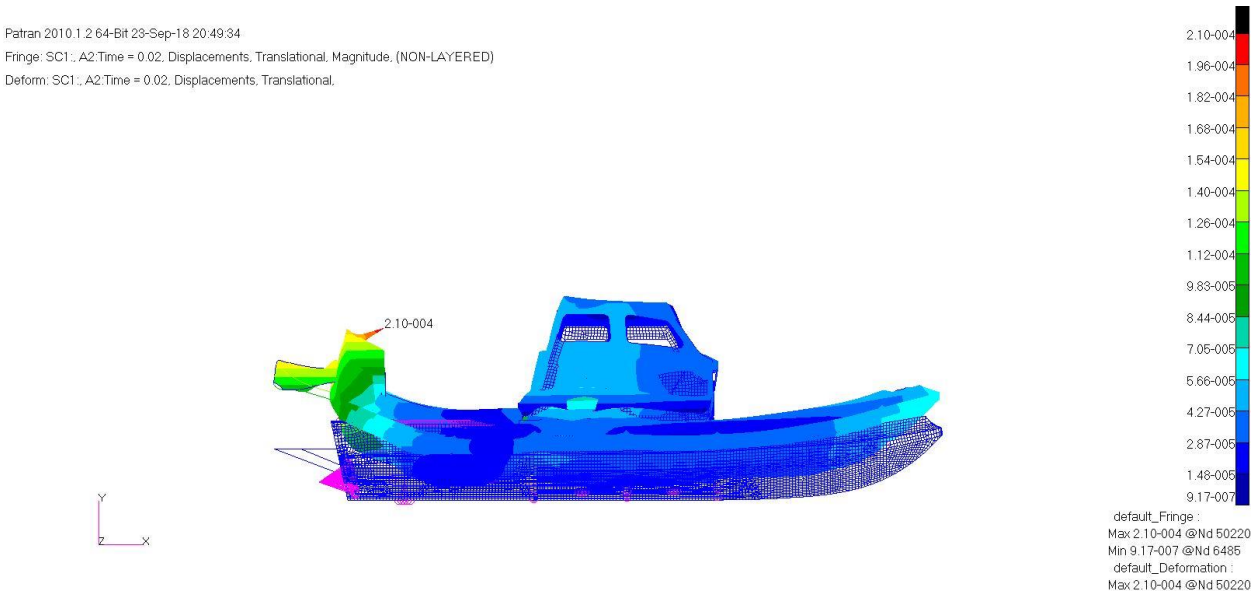

Figure C1. Side View of Deformation plot at 0.02 seconds

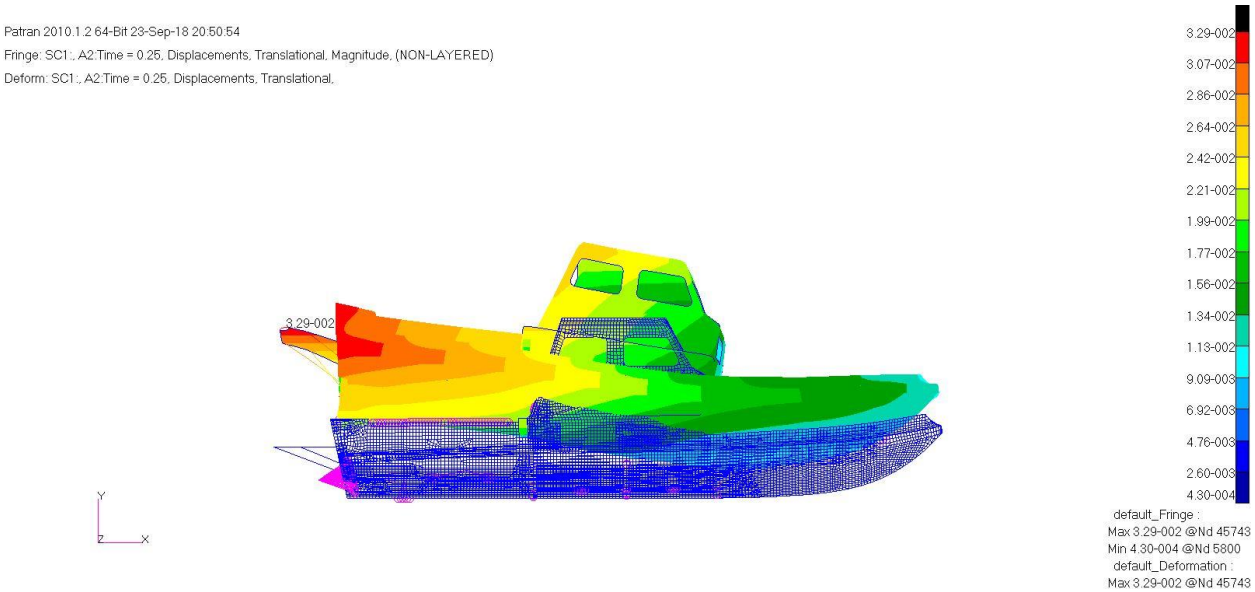

Figure C2. Side View of Deformation plot at 0.25 seconds

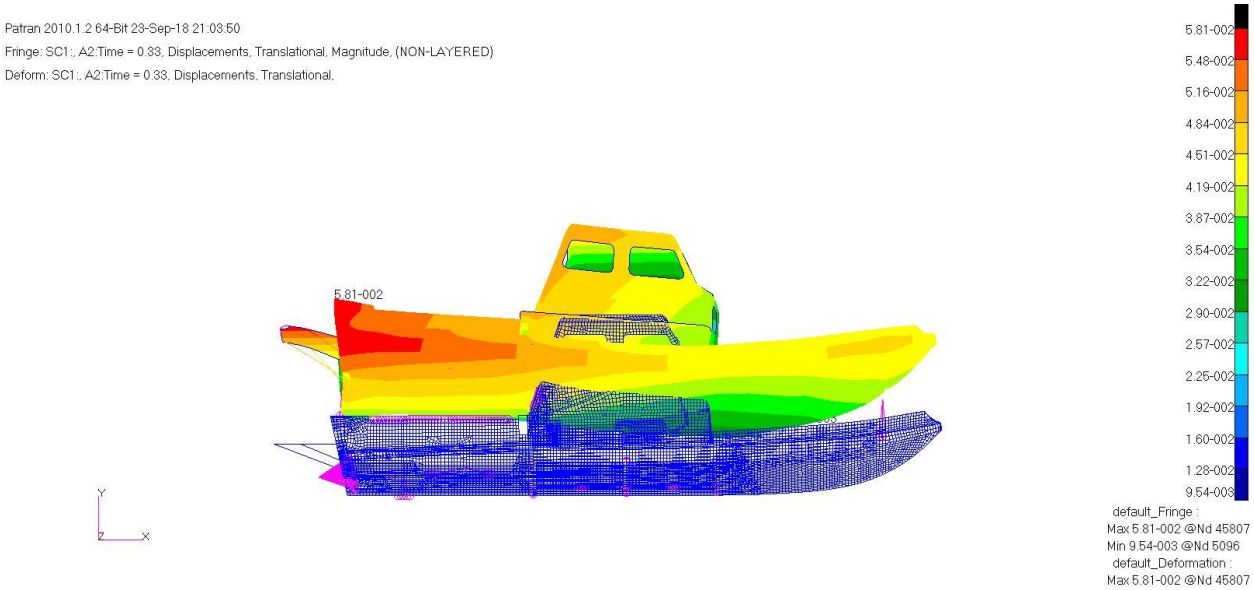

Figure C3. Side View of Deformation plot at 0.33 seconds

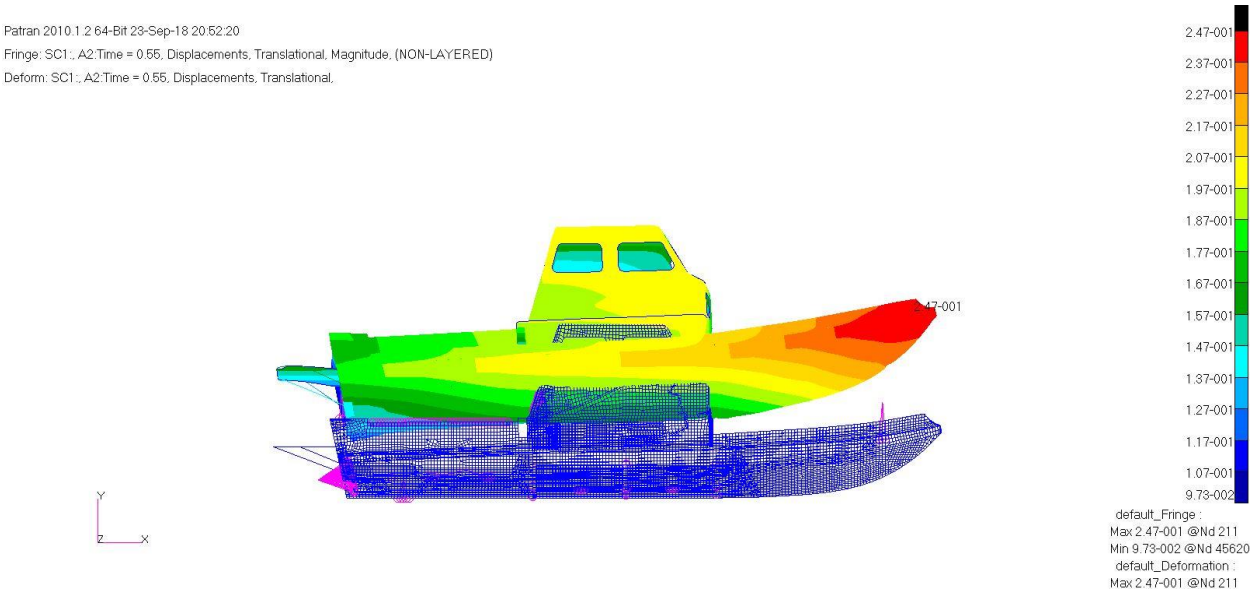

Figure C4. Side View of Deformation plot at 0.55 seconds

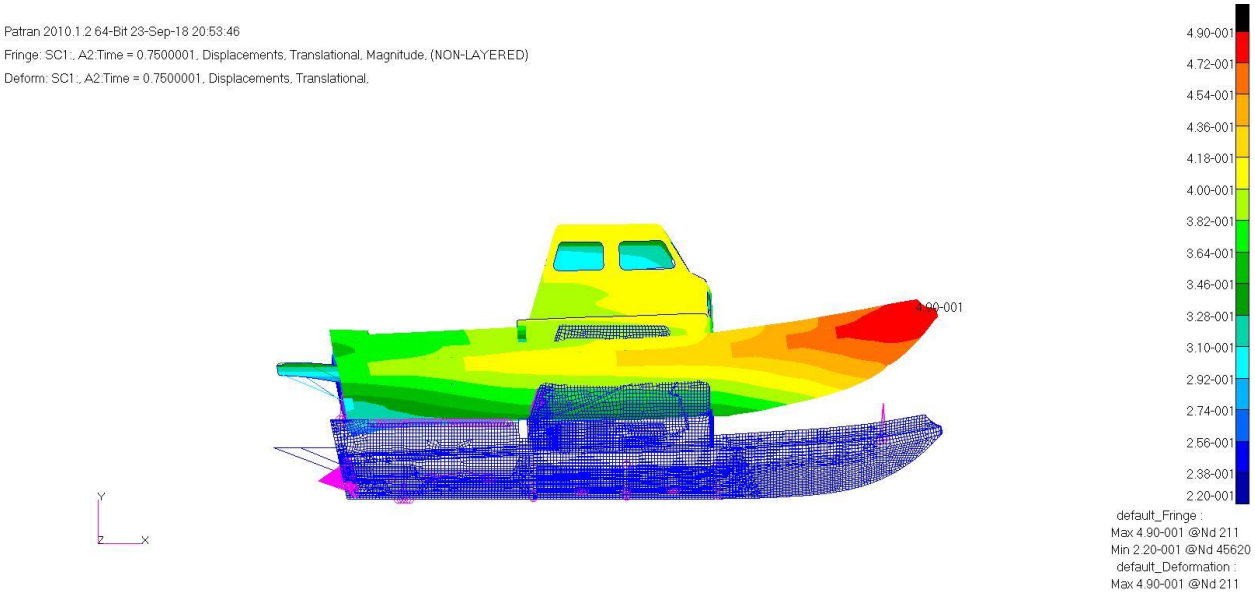

Figure C5. Side View of Deformation plot at 0.75 seconds

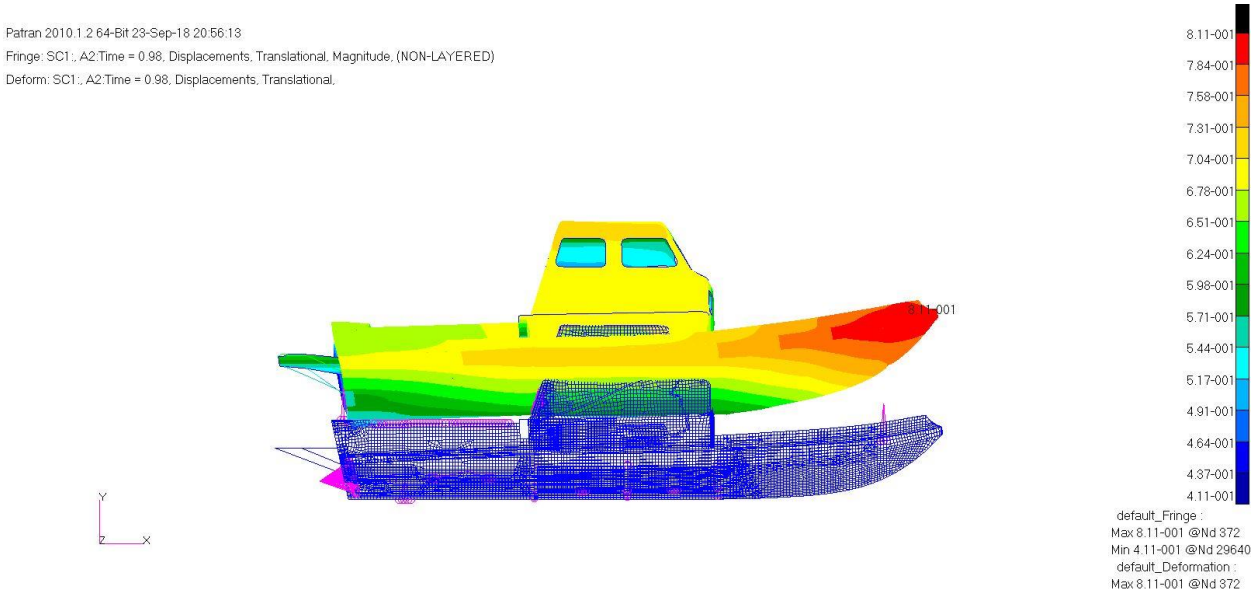

Figure C6. Side View of Deformation plot at 0.98 seconds

Appendix D – Approximation Validation Plots

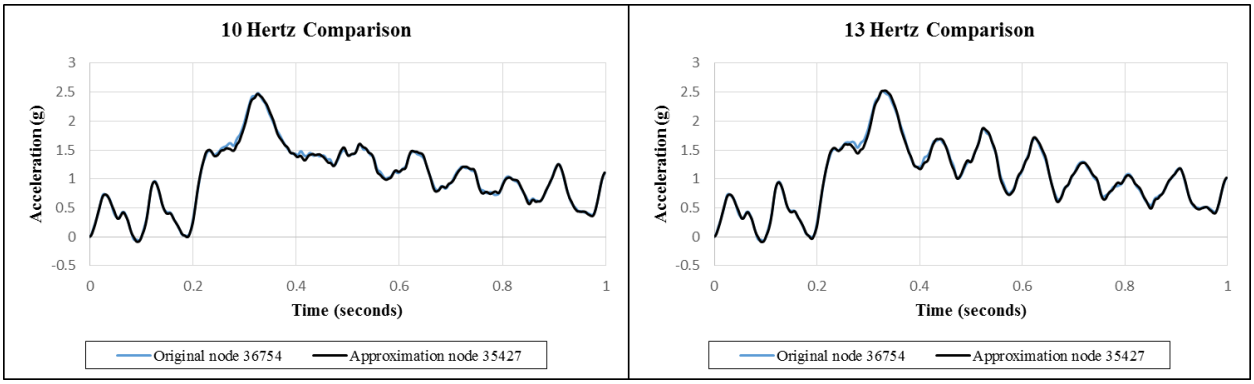

Figure D1. Original node 36754 versus Approximation node 35427 plot

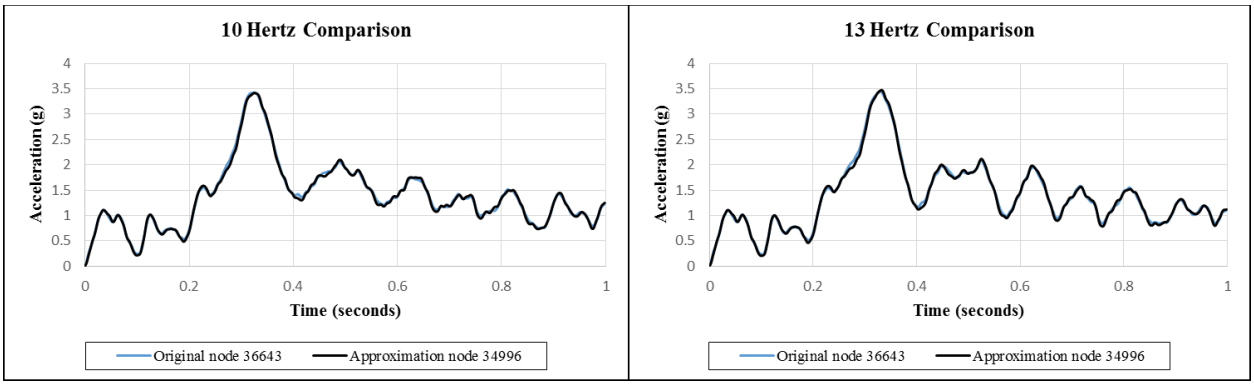

Figure D2. Original node 36643 versus Approximation node 34996 plot

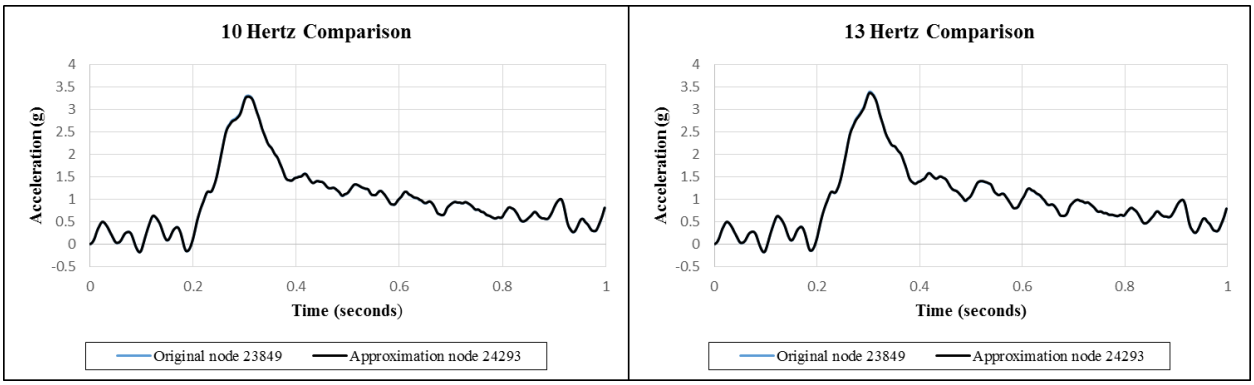

Figure D3. Original node 23849 versus Approximation node 24293 plot

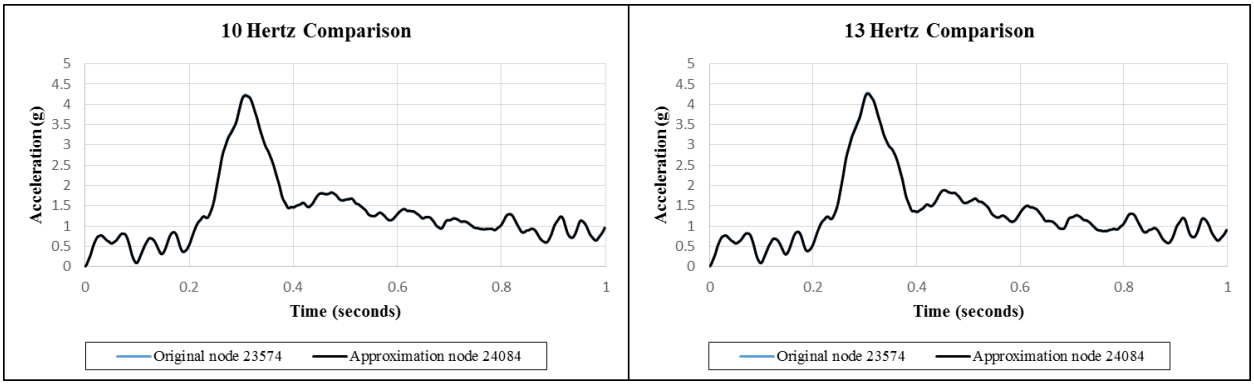

Figure D4. Original node 23574 versus Approximation node 24084 plot

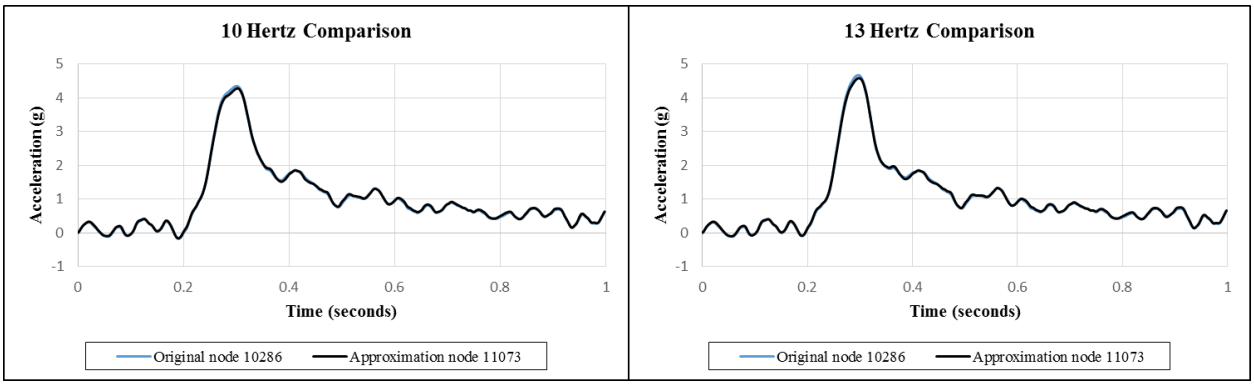

Figure D5. Original node 10286 versus Approximation node 11073 plot

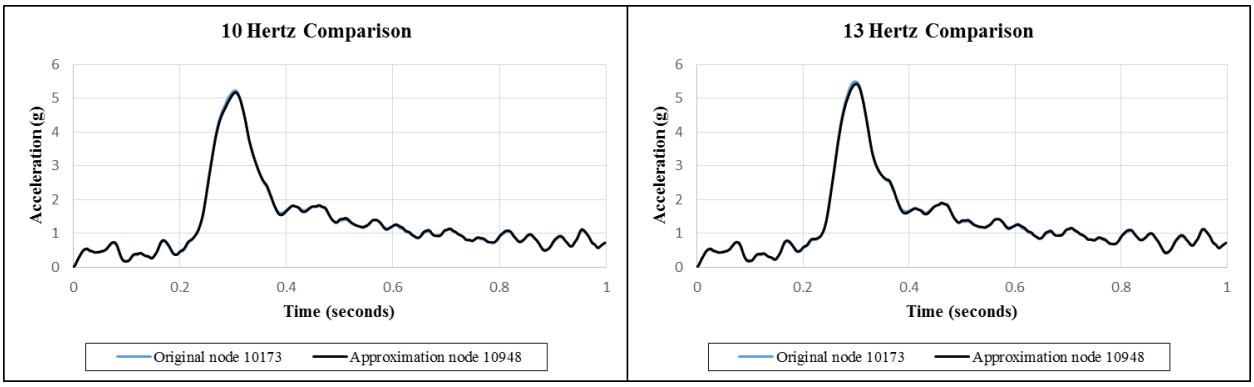

Figure D6. Original node 10173 versus Approximation node 10948 plot

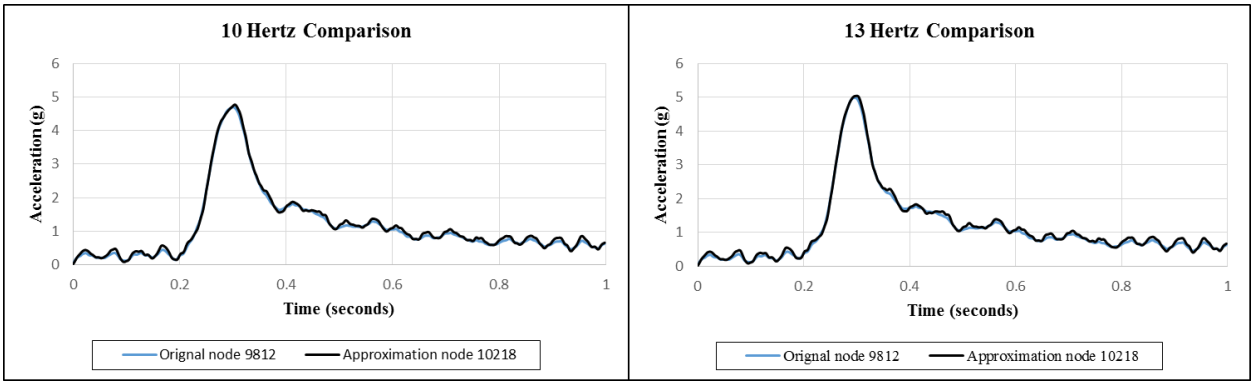

Figure D7. Original node 9812 versus Approximation node 10218 plot

VITA

Brian K. Johnson

C/O

Batten College of Engineering and Technology

1105 Engineering Systems Building

Norfolk, VA 23529

Cell Phone: (757) 270-8557, E-mail: bkeithjohn1@yahoo.com

Education: Old Dominion University, Mechanical Engineering, B.S., Dec. 2015

Old Dominion University, Mechanical Engineering, M.S., Dec. 2018

Professional Experience:

2016 – 2018 Naval Acquisition Development Program (NADP), Mechanical Engineer

2018 – Present NSWCDD DNA, Mechanical Engineer

Experience Summary:

As an NADP employee, I have worked at Naval Surface Warfare Center Dahlgren Division, Dam Neck Activity. Work has included rapid prototyping through the use of multiple Additive Manufacturing technologies, test planning, and test support.